

Nearly order from quantum disorder phenomena and its observation in the bosonic quantum anomalous Hall system

Fadi Sun and Jinwu Ye

Department of Physics and Astronomy, Mississippi State University, Mississippi State, Mississippi 39762, USA

Department of Physics, Capital Normal University, Beijing 100048, China

(Dated: March 12, 2024)

We report a new many body phenomena called "Nearly order from quantum disorder phenomena" (NOFQD). We demonstrate the NOFQD in the experimentally realized weakly interacting Quantum Anomalous Hall system of spinor bosons in an optical lattice. At a zero Zeeman field $h = 0$, there is a classically infinite degeneracy due to a spurious spin $SU(2)$ symmetry. By developing a systematic order from quantum disorder (OFQD) analysis, we find the quantum ground state to be a $N = 2$ XY-AFM superfluid (SF) state and also evaluate its excitation spectrum due to the effective potential generated by the OFQD at $h = 0$. At a high h , the system is in a Z-FM SF state. At a small $h > 0$, even there is no spurious symmetry anymore, there is still a delicate competition between the Zeeman field effect at $h > 0$ and the effective potential leading to a quantum phase transition between the two states. We name this novel many body phenomena as NOFQD which describes how a OFQD state response non-trivially to a small deformation. Starting from symmetry principle, we construct a Ginsburg-Landau (GL) type of effective action to investigate the nature of the transition. We establish intrinsic connections between the phenomenological GL theory and the microscopic calculations on the effective potential. Connections with the bilayer quantum Hall system with a total filling factor $\nu_T = 1$ are made. Some insightful analogy with $NAdS_2/NCFT_1$ (where N also means nearly) correspondence in the context of Sachdev-Ye-Kitaev models are hinted. Two types of OFQDs are classified, one response trivially, another non-trivially to a small deformation to the Hamiltonian leading to NOFQD. The NOFQD can be detected in the current cold atom bosonic quantum anomalous Hall experiments and may also appear in many other frustrated systems.

1. Introduction

The investigation and control of spin-orbit coupling (SOC) have become subjects of intensive research in both condensed matter and cold atom systems after the discovery of the topological insulators [1, 2]. In materials side, the SOC plays crucial roles in various 2d or layered insulators, semi-conductor systems, metals and superconductors without inversion symmetry. The quantum anomalous Hall (QAH) effect was experimentally realized in Cr doped $\text{Bi}(\text{Sb})_2\text{Te}_3$ thin films [3, 4]. In the cold atom side, using Raman schemes, several experimental groups [5–7] generated 2d SOC for neutral cold atoms in both continuum and in optical lattices. Especially, the bosonic analog of the QAH for spinor bosons ^{87}Rb was realized in [7], and the lifetime of SOC ^{87}Rb Bose-Einstein condensation (BEC) have been improved from 300 ms to 900 ms recently.

Motivated by the recent experiment on bosonic QAH [7], we investigate possible quantum many body phenomena in the bosonic quantum anomalous Hall (BQAH) model in a square lattice. In contrast to its fermionic counterpart, the bosonic QAH system is necessarily interacting. Most importantly, we discover a new many body phenomena we name "Nearly order from quantum disorder phenomena" (NOFQD). Our main results are presented in Fig.1. We achieve Fig.1 by the combination of specific microscopic calculations and the symmetry based phenomenological classification approaches.

We first perform microscopic calculations at weak in-

teraction limit and also identify its limitations. At a high Zeeman field h , we find the system is in a spin-polarized SF state along the z direction (named as Z-FM SF state). We evaluate the SF Goldstone mode at $\vec{k} = (0, 0)$ and the roton mode at $\vec{Q} = (\pi, \pi)$. We delineate the behaviour of the roton mode as h decreases: the roton mode continues to drop and eventually becomes a gapless quadratic mode $\sim v^2 k^2$ as $h \rightarrow 0^+$. At zero Zeeman field $h = 0$, we identify a spurious spin $SU(2)$ symmetry which leads to a classically infinitely degenerate ground state manifold. We develop a systematic order from quantum disorder (OFQD) analysis to determine an effective potential generated by the the OFQD effects. It selects the true quantum ground state from such a manifold to be a $N = 2$ XY-AFM SF state where $N = 2$ stands for the number of BEC momenta. It also opens a gap to the spurious quadratic roton mode. However, at any small $h > 0$, the spurious spin $SU(2)$ symmetry disappears, a simple classical analysis leads to a unique classical ground state which is the Z-FM SF. Although at a high h , the system is indeed in this Z-FM SF state, the classical picture may break down at a small $h > 0$. At a small $h > 0$, even there is not any spurious symmetries, there is still a delicate competition between the classical Z-FM SF state at a small $h > 0$ and the $N = 2$ XY-AFM superfluid (SF) state selected by the OFQD mechanism at $h = 0$ which may lead to a quantum phase transition between the two states. We name this new quantum many

body phenomena as "Nearly order from quantum disorder phenomena" (NOFQD) which happens slightly away from the conventional OFQD in the parameter space of a Hamiltonian. At the mean field level, we find that at a finite small h , the competition between the Zeeman energy and the effective potential first leads to a canted $N = 2$ XY-AFM SF state (CAFM), then drives a transition to the Z-FM state. Unfortunately, it becomes difficult to study the nature of the quantum phase transition from the microscopic weak coupling approach.

Then we change our strategy to symmetry based classification approach. Just from the constraints of the symmetries of the Hamiltonian, we construct a phenomenological Ginsburg-Landau (GL) type of effective action to investigate the NOFQD phenomena and the associated quantum phase transition from the a weak to strong Zeeman field. Using the GL action, we first find the excitations in the CAFM and Z-FM at low and high Zeeman field respectively which include the SF mode and the roton mode. It is the roton gap closing which drives the quantum phase transition from the CAFM to the Z-FM. Then by performing a renormalization group (RG) analysis, we find the transition is in the same universality class as the zero density Mott to superfluid transition, subject to a marginally and dangerously irrelevant $U(1)$ symmetry breaking (cubic) anisotropic term. So it has the critical exponents $z = 2, \nu = 1/2, \eta = 0$ subject to new logarithmic corrections. This $U(1)$ symmetry breaking cubic anisotropic term leads to experimentally observable logarithmic corrections to various scaling functions in the quantum critical regime.

By comparing our symmetry based GL action with the microscopic calculations at $h = 0$ and a high h , we establish the intrinsic and profound connections between the phenomenological GL theory and the microscopic calculations, especially the effective potential generated by the OFQD at $h = 0$, therefore endow the broad impacts of OFQD from a new and profound perspective. The microscopic calculations and the phenomenological GL theory are two different, but complementary approaches. Each has its own advantages and limitations. The combination of the two approaches lead to rather deep and complete understandings of the NOFQD phenomena in the bosonic QAH systems. We also make instructive mappings between the GL theory here and the Chern-Simon GL theory applied by one of the authors to study the exciton superfluid and quantum phase transitions (QPT) in the bilayer quantum Hall systems at the total filling factor $\nu_T = 1$. The scaling behaviours of various physical quantities such as the roton gaps, the specific heat, transverse magnetization and the Lyapunov exponent/butterfly velocity are derived.

In the conclusion section, in order to spell out the crucial connections and differences between the OFQD and NOFQD, we classify the OFQD into two classes: Type-I responses trivially to a deformation λ , type-II does non-

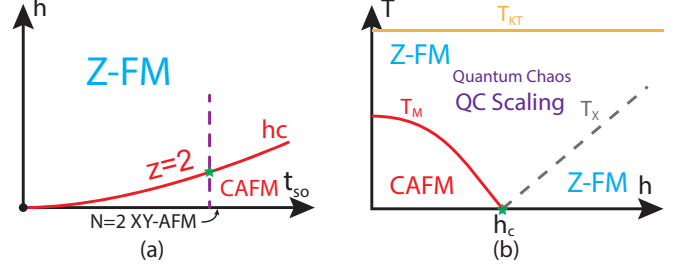


FIG. 1. The quantum phase transition associated due to the "Nearly order from quantum disorder phenomena" NOFQD phenomena in the interacting bosonic QAH system (a) Zero temperature phase diagram [8] as a function of t_{so}/t_0 and h/t_0 with a fixed n_0U . The CAFM SF phase is labeled by $\langle\psi_1\rangle \neq 0, \langle\psi_2\rangle \neq 0$, while the Z-FM SF phase labeled by $\langle\psi_1\rangle \neq 0, \langle\psi_2\rangle = 0$ or the other way around. The quantum phase transition is in the same universality class as the zero-density SF to Mott transition subject to the dangerously marginally irrelevant cubic anisotropic term described by Eq.32. (b) Finite temperature phase diagram in the (h, T) plane with fixed t_{so}/t_0 and n_0U (along the dashed line in (a)). Only the part below $T < T_{KT}$ is shown. The dashed line $T_X \sim \Delta_R$ scales as the roton gap and stands for the crossover from the QC regime to the gapped regime in the Z-FM SF phase.

trivially and leads to the NOFQD. Some interesting and insightful analogy with $NAdS_2/NCFT_1$ (where N also means nearly) correspondence in the context of Sachdev-Ye-Kitaev models are also hinted. The ongoing experimental efforts to detect these novel NOFQD phenomena are critically examined. Some future perspectives are outlined.

The rest of the paper is organized as into 4 parts. In part I consisting of Sec.2-5, we perform microscopic calculations at $h = 0$ and strong $h \gg U$ at weak coupling limit. In part II consisting of Sec.6-9, to capture the NOFQD, we perform phenomenological effective action calculations at any h at weak coupling limit. Then in Part III consisting of Sec.10-11, we contrast the phenomenological effective action calculations in part II with the microscopic calculations in part I, therefore establish the intrinsic connections between the two complementary approaches. We discuss the experimental implications and reach conclusions in Sec.12 and 13 respectively.

2. The classical ground state at a high field $h \gg U$ and its possible breakdown in the small $h \lesssim U$ limit.

The experimentally realized quantum anomalous Hall model of spinor bosons in a square lattice is described by the Hamiltonian [7]

$$\mathcal{H} = -t_0 \sum_{\langle ij \rangle} a_i^\dagger \sigma^z a_j + it_{so} \sum_{\langle ij \rangle} a_i^\dagger (\mathbf{d}_{ij} \cdot \vec{\sigma}) a_j - h \sum_i a_i^\dagger \sigma^z a_i + \frac{U}{2} \sum_i n_i(n_i - 1) - \mu \sum_i n_i \quad (1)$$

where $a_i = (a_{i\uparrow}, a_{i\downarrow})^\top$ and $\langle ij \rangle$ denotes a pair of nearest neighbor sites, and $\mathbf{d}_{ij} = \mathbf{r}_i - \mathbf{r}_j$. U is the repulsive onsite interaction, and μ is the chemical potential, $\sigma_{x,y,z}$ are three Pauli matrices, and $n_i = a_i^\dagger a_i$ is the number of particles on site- i . For the ^{87}Rb atoms used in the recent experiment [7], the two pseudo-spin components $\sigma = \uparrow, \downarrow$ denote the two hyperfine states $|F = 1, m_F = 0\rangle$ and $|F = 1, m_F = -1\rangle$.

The Hamiltonian has the particle number conservation $U_c(1)$ symmetry, and a spin-orbital coupled $[C_4 \times C_4]_D$ symmetry. Under the mirror transformation $\mathcal{M} = (-1)^i R_z(\pi) \mathcal{T}$, $h \rightarrow -h$, so $h = 0$ has an enlarged Mirror symmetry. So we only need to focus on $h \geq 0$ cases. In this Letter, we focus on the experimentally accessible regime $0 \leq t_{\text{so}} \leq t_0$ and $U/t_0 \ll 1$. The global phase diagram in most general parameter space will be worked out in a much longer version [9].

Any small $h > 0$ breaks the mirror symmetry and split the two degenerate single-particle states at momentum $(0, 0)$ and (π, π) . A straightforward mean field analysis predicts the condensation occurs at either $(0, 0)$ or (π, π) depending on the sign of h . Due to its spin alinement along the z axis, we name it Z-FM superfluid in Fig.1.

When the spectrum minimum is located at $(0, 0)$ or (π, π) , the non-interacting Hamiltonian takes a simple form

$$H_0(k) = -[h + 2t_0(\cos k_x + \cos k_y)]\sigma_z \quad (2)$$

where the SOC t_{so} drops out.

Let us consider $h > 0$ case, thus the minimum is located at $(0, 0)$. In the weak coupling limit $U/t \ll 1$, by writing

$$a_{k\uparrow} \rightarrow \sqrt{N_0}\delta_{k,0} + \psi_{k\uparrow}, \quad a_{k\downarrow} \rightarrow \psi_{k\downarrow} \quad (3)$$

where N_0 is the number of condensate atoms, and N_s is the total number of lattice sites, thus $n_0 = N_0/N_s$ is the condensate fraction.

We can perform the expansion $\mathcal{H} = \mathcal{H}^{(0)} + \mathcal{H}^{(1)} + \mathcal{H}^{(2)} + \dots$ where the superscript denotes the order in the quantum fluctuations. The zeroth order term $\mathcal{H}^{(0)} = E_0 = -\frac{1}{2}Un_0N_0$ is the classical energy of the condensate. The vanishing of the linear term sets the value of the chemical potential $\mu = -h - 4t_0 + Un_0$. Diagonalizing $\mathcal{H}^{(2)}$ by a generalized 4×4 Bogliubov transformation leads to:

$$H = E_0 + E_0^{(2)} + \sum_{k,s=\pm} \omega_s(k)(\alpha_{sk}^\dagger \alpha_{sk} + 1/2) \quad (4)$$

where $E_0^{(2)} = -(h + 4t_0 + \frac{1}{2}Un_0)$ and $\omega_\pm(k)$ are the two Bogliubov modes.

Since $\omega_+(\mathbf{k}) > \omega_-(\mathbf{k})$ always holds, so we focus on $\omega_-(\mathbf{k})$ which displays a gapless superfluid Goldstone mode near $\mathbf{k} = (0, 0)$ and a gapped roton mode at $\mathbf{k} = (\pi, \pi)$. In the long wavelength limit, we find the

superfluid Goldstone mode becomes linear $\omega_-(k) = c|\mathbf{k}|$ where the SF velocity is

$$c = \sqrt{\frac{2(4t_0^2 - 2t_{\text{so}}^2 + th)Un_0}{4t_0 + h}} \quad (5)$$

which is shown in Fig.2a. In the $h \rightarrow 0$ limit, it reduces to $c = \sqrt{n_0Ut(2 - t_s^2/t^2)}$.

In Fig.2a, at a fixed $t_{\text{so}} = 1$, as h decreases to 0 sitting on the boundary between Z \uparrow FM-SF at $(0, 0)$ and the Z \downarrow FM-SF at (π, π) , the roton mode gets lower and lower, then touches zero at $\tilde{Q} = (\pi, \pi)$. In the $h \rightarrow 0$ limit, the roton mode can be extracted from $\omega_-(k)$ mode near $k = (\pi, \pi) + q$:

$$\omega_-(k) = \sqrt{4h^2 + v_4(q_x^2 + q_y^2)^2} \quad (6)$$

where

$$v_4 = \frac{(2t_0^2 - t_{\text{so}}^2)[t_0(4t_0 + n_0U) - 2t_{\text{so}}^2]}{2t_0(4t_0 + n_0U)} \quad (7)$$

which depends on the the interaction n_0U .

In the weak coupling limit $n_0U \ll t_0$, the v_4 can be simplified as $v_4 = (2t_0^2 - t_{\text{so}}^2)^2/(4t_0^2) = (v^2)^2$ which remains finite even at the non-interacting limit $n_0U = 0$. In the small h limit, the roton gap

$$\Delta_R^0(h) = 2|h| \quad (8)$$

which is independent of t_{so} and shown in the dashed line in Fig.4b.

As one decreases h from $h \gg U$ to $h \lesssim U$, then to 0^+ , the roton mode gets lower and lower, then touches zero at $h = 0^+$, it reduces to the quadratic form $\omega_-(k) = \sqrt{v_4(q_x^2 + q_y^2)^2} = v^2q^2$. This behaviour may signify a possible first order transition at $h_c = 0^+$. This physical picture leads to the naive phase diagram shown in Fig.S1 in SM. However, as to be shown below, this naive physical picture only holds when h is sufficiently large $h > U$, but may break down [13] at a small $h \lesssim U$.

3. The order from quantum disorder (OFQD) effects to determine the quantum ground state at $h = 0$.

The single-particle energy spectrum $U = 0$ of Eq.(1) in the momentum space can be easily obtained: $\epsilon_{\pm, \mathbf{k}}^h = \pm \sqrt{[h + 2t_0(\cos k_x + \cos k_y)]^2 + 4t_{\text{so}}^2(\sin^2 k_x + \sin^2 k_y)}$. At $h = 0$, its lower branch develops two degenerate minima at momentum $(0, 0)$ and (π, π) , and two eigen-spinors are $\eta_0 = (1, 0)^\top$ and $\eta_\pi = (0, 1)^\top$ respectively. There is a classically degenerate family of states:

$$\Psi_i = c_0\eta_0 + (-1)^{i_x+i_y}c_\pi\eta_\pi \quad (9)$$

where the two complex number c_0 and c_π satisfy normalization condition $|c_0|^2 + |c_\pi|^2 = 1$. This classically

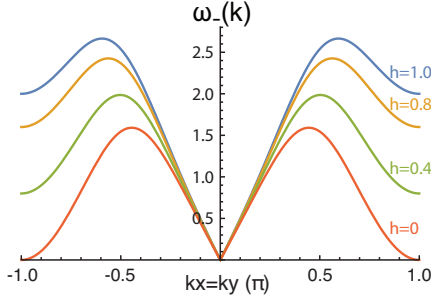


FIG. 2. The Critical Behaviour of the superfluid Goldstone mode $\omega_{-}(k_x = k_y)$ starting at $(t_{so}/t_0 = 1, h/t_0 = 1)$. Decreasing h/t from 1 to 0, the roton at $\vec{Q} = (\pi, \pi)$ gets lower and lower and drops to zero at $h = 0$ signifying a possible (in fact, naive) first order transition.

degenerate manifold is due to the spurious $SU(2)_s$ symmetry at the mean field level.

By writing the spinor field as $\Psi = \sqrt{N_0}\Psi_0 + \psi$, we can expand the Hamiltonian $\mathcal{H} = \mathcal{H}^{(0)} + \mathcal{H}^{(1)} + \mathcal{H}^{(2)} + \dots$. The zeroth order term $\mathcal{H}^{(0)}$ gives the classical ground state energy $E_0 = -\frac{1}{2}Un_0N_0$. Setting the linear term $\mathcal{H}^{(1)}$ vanish gives the value of the chemical potential $\mu = -4t + Un_0$. Diagonalizing the quadratic term $\mathcal{H}^{(2)}$ by a generalized 8×8 Bogliubov transformation [10] leads to:

$$\mathcal{H} = E_0 + E_{\text{ofd}} + \sum_{l, \mathbf{k} \in RBZ} \omega_{l, \mathbf{k}} \alpha_{l, \mathbf{k}}^\dagger \alpha_{l, \mathbf{k}} \quad (10)$$

where $E_{\text{ofd}} = -(4t_0 + \frac{1}{2}n_0U)N_s + \frac{1}{2} \sum \omega_{l, \mathbf{k}}$ is quantum correction to the mean field ground-state energy, and $\omega_{l, \mathbf{k}}$ with $l = 1, \dots, 4$ represent 4 Bogliubov spectrum.

It is convenient to parameterize c_0 and c_π as

$$c_0 = e^{-i\phi/2} \cos(\theta/2), \quad c_\pi = e^{i\phi/2} \sin(\theta/2) \quad (11)$$

then we can plot numerically $E_{\text{ofd}}(\theta, \phi)$ as a function of θ and ϕ in Fig.2 where one can identify the quantum ground states as $\theta = \pi/2$ and $\phi_m = \pi/4 + m\pi/2$ ($m = 0, 1, 2, 3$). It has a uniform density $\langle n_i \rangle = n_0$ and a XY-AFM ordered spin structure: $\langle a_i^\dagger \vec{\sigma} a_i \rangle = (-1)^{i_x+i_y} n_0 (\cos \phi_m, \sin \phi_m, 0)$. It is 4 fold degenerate breaking the joint C_4 symmetry.

After identifying the quantum ground-state as the $N = 2$ XY-AFM SF state, we can also evaluate all $\omega_{1,2,3,4}(k)$ in Eq.10. There are one linear $\omega_1 \sim k$ SF Goldstone mode and one $\omega_2 \sim k^2$ quadratic roton mode located at $(0, 0)$. While $\omega_3(k)$ and $\omega_4(k)$ are two fully gapped higher energy modes.

4. The Roton mass gap generated from the OFQD mechanism in the $N = 2$ XY-AFM state at $h = 0$.

Now we can have a better understanding of the spurious $SU(2)_s$ symmetry and the origin of this spurious quadratic roton mode: Indeed, it setting the two minima

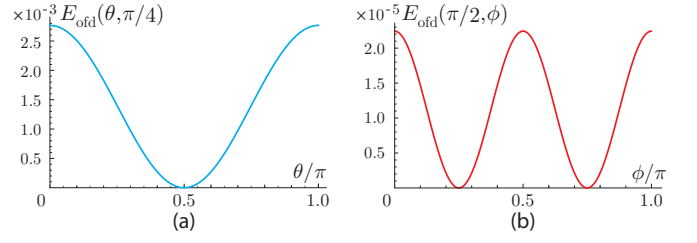


FIG. 3. The quantum ground-state energy density near its minimum at (a) $\theta = \pi/2$ at fixed $\phi = \pi/4$, (b) $\phi = \pi/4, 3\pi/4$ at fixed $\theta = \pi/2$ where the coefficients A and B can be extracted respectively. We used $n_0U/t_0 = 1$ and $t_{so}/t_0 = 1$. Despite both A and B are generated by the OFQD, the numerical value of A is larger than B by 2 orders of magnitude.

$(0, 0)$ and (π, π) into the kinetic energy, then the term involving t_{so} drops out, so at the mean field level, the system has the $SU(2)_s$ symmetry originating from the exact $SU(2)_s$ symmetry at $t_{so} = 0$. While the $N = 2$ XY-AFM state is a collinear state invariant under the rotation $e^{i\alpha \vec{\sigma} \cdot \vec{n}}$, $\vec{n} = (1, 1, 0)$, in fact, it is a XY-FM state in the rotated $\tilde{S}U(2)$ basis $\tilde{\mathbf{S}}_i = ((-1)^{i_x+i_y} S_i^x, (-1)^{i_x+i_y} S_i^y, S_i^z)$ where the $SU(2)_s$ symmetry is manifest (See appendix B). So its breaking to the FM state leads to the spurious quadratic FM roton mode which is remanent of the exact FM mode at $t_{so} = 0$. However, the OFQD opens a gap to this spurious quadratic FM roton mode.

The OFQD mechanism picks up $\theta = \pi/2$ and $\phi = \pi/4$ as the quantum ground state. Then we can expand the ground-state energy around the minimum as [2]:

$$E_{\text{GS}}[\theta, \phi] = E_0 + \frac{A}{2} \delta\theta^2 + \frac{B}{2} \delta\phi^2 \quad (12)$$

where $\theta = \pi/2 + \delta\theta$ and $\phi = \pi/4 + \delta\phi$, the two coefficients $A \sim (n_0U)^2/t$ and $B \sim (n_0U)^4/t$ can be extracted from Fig.M2.

Using the commutation relations $[\frac{1}{2}n_0\delta\theta, \delta\phi] = i\hbar$, one can see that the "quantum order from dis-order" mechanism generates a roton gap:

$$\Delta_R(h = 0) = 2\sqrt{AB}/n_0 \quad (13)$$

which is the dashed line in Fig.M3b (also in the Fig.S1b in SM). The SF Goldstone mode remains unaffected due to its protection by the $U(1)$ symmetry breaking.

5. The nearly order from quantum disorder (NOFQD) effects at a small $0 < h \lesssim U$: Mean field theory treatment in the microscopic calculation

Any small $h > 0$ spoils the spurious $SU(2)_s$ symmetry and also splits the degenerate single-particle state at momentum $(0, 0)$ and (π, π) . So one can determine the ground state to be the classical Z-FM SF state even at an infinitesimal small h . However, when $h \lesssim U$, the splitting is so small that any small interaction U still mix the two states considerably. So even the spurious $SU(2)_s$ symmetry disappears at any small h , one must still take into

account the OFQD effects at $h = 0$ and study the delicate competition between the OFQD generated effective potential in Fig.2 due to the interaction U with the Zeeman energy due to a small finite h . We call this phenomena as NOFQD.

As shown in SM, the OFQD generated effective potential in Fig.2 can be cast into the form:

$$E_{\text{ofd}} = E_{\text{ofd},0} + N_s \left[\frac{1}{4} A (1 + \cos 2\theta) + \frac{1}{64} B (1 - \cos 2\theta)^2 (1 + \cos 4\phi) + \dots \right]. \quad (14)$$

Appealingly, one can cast the energy density: $\mathcal{E}_{\text{ofd}} = E_{\text{ofd}}/N_s$ into a compact form

$$\mathcal{E}_{\text{ofd}} = \frac{1}{2} A (|c_0|^2 - |c_\pi|^2)^2 + \frac{1}{2} B [(c_0 c_\pi^*)^2 + (c_0^* c_\pi)^2] \quad (15)$$

where the coefficients A and B are positive numbers at least in the weak coupling limit.

To get to finite temperatures, it is necessary to parameterize the quantum fluctuations in the polar coordinate as:

$$a_i(\tau) = \sqrt{n_i(\tau)} e^{i\chi_i(\tau)} [c_{0,i}(\tau)\eta_0 + (-1)^i c_{\pi,i}(\tau)\eta_\pi] \quad (16)$$

and write the action as two parts $\mathcal{S} = \int d\tau (\mathcal{L} + \delta\mathcal{L}_c)$.

$$\mathcal{L} = \sum_{\mathbf{k}} \bar{a}_{\mathbf{k}} [\partial_\tau + \epsilon_{-\mathbf{k}}^{h=0} - \mu] a_{\mathbf{k}} + \frac{U}{2} \sum_i n_i (n_i - 1) \\ \delta\mathcal{L}_c = \sum_i [\mathcal{E}_{\text{ofd}}(c_{0,i}, c_{\pi,i}) - nh(|c_{0,i}|^2 - |c_{\pi,i}|^2)] \quad (17)$$

where the second part contains the competition between the order-from-disorder effects generated effective potential and the Zeeman effect

With the parametrization Eq.(11), we obtain

$$\mathcal{L}_0 = E_0 + \frac{A}{2} \cos^2 \theta + \frac{B}{8} \sin^4 \theta \cos^2 2\phi - n_0 h \cos \theta \quad (18)$$

where E_0 is independent of θ and ϕ . The $\cos 4\phi$ term is a result of C_4 symmetry and plays a similar role as the C_4 clock term. Performing a minimization with respect to θ and ϕ leads to $\theta_0 = \arccos(h/h_c)$ and $\phi_0 = \pi/4$ with $h_c = A/n_0$. In the $h \rightarrow 0^+$ limit, one recovers the $N = 2$ XY-AFM SF state. For $0 < h < h_c$, the spin-orbital structure is $n_0((-1)^{i_x+i_y} \sin \theta_0 \cos \phi_0, (-1)^{i_x+i_y} \sin \theta_0 \cos \phi_0, \cos \theta_0)$, and named as a canted AFM (CAFM) SF state. When $h \leq h_c$, the spin structure becomes $n_0(0, 0, 1)$ which is fully aligned to the z direction, so named the Z-FM state (Fig.3a).

Unfortunately, in this microscopic NOFQD calculation, the BEC condensation density n_0 is taken as a constant at very beginning (see above Eq.10). The chemical potential $\mu = -h - 4t + U n_0$ also depends on n_0 and h . It is very difficult to capture the density fluctuations in a

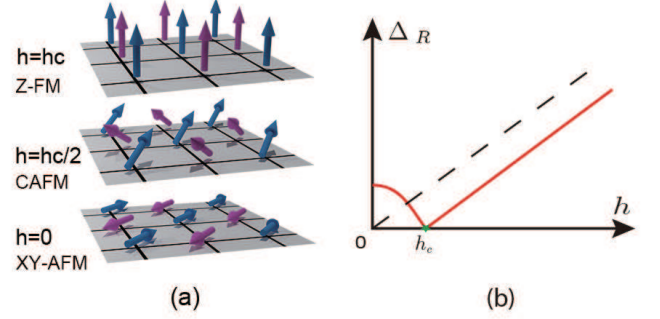


FIG. 4. (a) The spin-bond structure of the ground-state as the Zeeman field h from 0 to h_c and beyond. (b) The Roton gap Δ_R from the second equation in Eq.27 below h_c and Eq.31 above h_c through a 2nd QPT. The dashed line is the roton gap Eq.8 calculated by the naive Bogliubov calculation.

consistent way. To study the competition between the effective potential generated by the OFQD and the Zeeman field, then to capture the nature of the quantum phase transition near $h \sim h_c$, one must take account the density fluctuations. To circumvent this difficult suffered in this this microscopic NOFQD calculation, one may turn to an independent phenomenological calculations based on the symmetries of the Hamiltonian.

6. Ginsburg-Landau type action from the symmetry principle to study the NOFQD phenomena:

To capture the density fluctuations in a consistent way, it is convenient to absorb the density/phase part into c_0 and c_π in Eq.16 and re-parameterize low energy quantum fluctuations at a small $h \ll U$ as

$$a_{i\alpha} = \psi_1 \eta_0 + (-1)^i \psi_2 \eta_\pi \quad (19)$$

which includes both spin and charge fluctuations.

Then one can find the density $n = |\psi_1|^2 + |\psi_2|^2$ and the spin:

$$S^+ = (-1)^i \psi_1^* \psi_2, \\ S^- = (-1)^i \psi_2^* \psi_1, \\ S^z = |\psi_1|^2 - |\psi_2|^2 \quad (20)$$

Note that here we only expand the boson field in terms of the two minima of the kinetic term without assuming any symmetry breaking. In order to study the transition from the weak coupling SF to the strong coupling Mott phase an an integer filling, we construct the Ginsburg-Landau action consistent with all the symmetries of the Hamiltonian such as the translational symmetry, the $U(1)_c$ symmetry, the $[C_4 \times C_4]_D$ (or $[R_{\pi/2} \times R_{\pi/2}]_D$) spin-orbital coupled symmetry and the Mirror symmetry

\mathcal{M} at $h = 0$:

$$\begin{aligned} \mathcal{L} = & \psi_1^* \partial_\tau \psi_1 + \psi_2^* \partial_\tau \psi_2 + v^2 (|\nabla \psi_1|^2 + |\nabla \psi_2|^2) \\ & + r(|\psi_1|^2 + |\psi_2|^2) + \frac{U}{2} (|\psi_1|^2 + |\psi_2|^2)^2 \\ & + \frac{A}{2} (|\psi_1|^2 - |\psi_2|^2)^2 + \frac{B}{2} [(\psi_1^* \psi_2)^2 + (\psi_1 \psi_2^*)^2] \\ & - h(|\psi_1|^2 - |\psi_2|^2) + \dots \end{aligned} \quad (21)$$

where the \dots means the higher order terms consistent with all the symmetries (see SM Eq.S25), $r < 0$ ensures the system is always in a superfluid phase, and v, U are all positive to make the system stable. However, the sign of A and B can not be determined by the symmetry analysis, but can be fixed by comparing with the microscopic calculations at the weak coupling limit. The last h term is the Zeeman field coupled to S^z in Eq.20. It breaks the Mirror symmetry \mathcal{M} . The relations between these phenomenological parameters and the microscopic ones calculated in the previous sections will be established in Sec.9.

Although this effective action was designed to study the transition from weak coupling to the strong coupling. Here, we only use it to study the transition driven by the Zeeman field, while leave the original goal to a future study [31].

It is convenient to write the two bosons in terms of its magnitude and phase $\psi_\alpha = \sqrt{\rho_\alpha} e^{i\theta_\alpha}$, then

$$\begin{aligned} \Omega = & r(\rho_1 + \rho_2) + \frac{U}{2}(\rho_1 + \rho_2)^2 + \frac{A}{2}(\rho_1 - \rho_2)^2 \\ & + 2B\rho_1^2\rho_2^2 \cos^2[2(\theta_1 - \theta_2)] - h(\rho_1 - \rho_2) \end{aligned} \quad (22)$$

which leads to two sets of saddle point solutions.

For $h < h_c = -rA/U = \rho_0 A$:

$$\begin{aligned} \bar{\rho}_1 = & (\rho_0 + h/A)/2, \quad \bar{\rho}_2 = (\rho_0 - h/A)/2, \\ \theta_1 - \theta_2 = & \pi/4 + m\pi/2, \quad m = 0, 1, 2, 3 \end{aligned} \quad (23)$$

where $\rho_0 = \bar{\rho}_1 + \bar{\rho}_2 = -r/U$ is the total density of the spinor atoms [32]. Note that at these saddle points, the effective mass term $r = -\rho_0 U$ is independent of h . From Eq.20, $S^z = \bar{\rho}_1 - \bar{\rho}_2 = h/A = \rho_0 \cos \theta_0$, namely, $\cos \theta_0 = h/h_c$. So the saddle point Eq.23 has the spin-orbital structure $\rho_0((-1)^{i_x+i_y} \sin \theta_0, (-1)^{i_x+i_y} \sin \theta_0, \cos \theta_0)$ named as a canted AFM (CAFM) SF state (Fig.3a). In the $h \rightarrow 0^+$ limit, it reduces to the the $N = 2$ XY-AFM SF state with $\theta_0 = \pi/2$. When $h \rightarrow h_c^-$, the spin structure becomes $n_0(0, 0, 1)$ which is fully aligned to the z direction, so named the Z-FM state (Fig.3a).

For $h > h_c$:

$$\bar{\rho}_1 = \rho_0, \quad \rho_2 = 0 \quad (24)$$

which, according to Eq.20, is the Z-FM state with $\theta_0 = 0$ in Fig.3a. Note that at this saddle points, the effective

mass term $r = h - \rho_0(A + U) = (h - h_c) - \rho_0 U$ depends on h and $\lim_{h \rightarrow h_c^+} r = -\rho_0 U$ which approaches to the same value as that at $h \leq h_c$.

At the mean field level, we reproduced the two different ground states $h < h_c$ and $h > h_c$ respectively achieved by the microscopic approach used in the previous sections. In the following, we will explore the quantum fluctuations, especially the Quantum phase transition between the two.

7. The canted anti-ferromagnetic (CAFM) SF phase at $h < h_c$.

Below the critical point $h < h_c$, the bosonic system is in canted anti-ferromagnetic superfluid phase Eq.23. Without of loss generality, we choose $\bar{\theta}_1 = 0$ and $\bar{\theta}_2 = \pi/4$ and write fluctuations as $\psi_\alpha = \sqrt{\bar{\rho}_\alpha + \delta\rho_\alpha} e^{i(\bar{\theta}_\alpha + \delta\theta_\alpha)}$, for the notation simplicity, we drop the δ in $\delta\theta_\alpha$, then

$$\begin{aligned} \mathcal{L}_{\text{CA}} = & i\delta\rho_1 \partial_\tau \theta_1 + i\delta\rho_2 \partial_\tau \theta_2 + v^2 \bar{\rho}_1 (\nabla \theta_1)^2 + v^2 \bar{\rho}_2 (\nabla \theta_2)^2 \\ & + \frac{U}{2} (\delta\rho_1 + \delta\rho_2)^2 + \frac{A}{2} (\delta\rho_1 - \delta\rho_2)^2 + 8B\bar{\rho}_1^2 \bar{\rho}_2^2 (\theta_1 - \theta_2)^2 \\ & + \frac{v^2}{4\bar{\rho}_1} (\nabla \delta\rho_1)^2 + \frac{v^2}{4\bar{\rho}_2} (\nabla \delta\rho_2)^2 \end{aligned} \quad (25)$$

where we still keep the gradient term on the density fluctuations in the 3rd line which are higher orders to the mass terms of the density fluctuations in the second line [33].

Following bilayer quantum Hall systems [28–30], we introduce $\bar{\rho}_\pm = \bar{\rho}_1 \pm \bar{\rho}_2$, $\delta\rho_\pm = \delta\rho_1 \pm \delta\rho_2$ and $\theta_\pm = \theta_1 \pm \theta_2$, then

$$\begin{aligned} \mathcal{L}_{\text{CA}} = & \frac{i}{2} \delta\rho_+ \partial_\tau \theta_+ + \frac{i}{2} \delta\rho_- \partial_\tau \theta_- + \frac{v^2 \rho_0}{4} [(\nabla \theta_+)^2 + (\nabla \theta_-)^2] \\ & + \frac{U}{2} (\delta\rho_+)^2 + \frac{A}{2} (\delta\rho_-)^2 + \frac{B}{2} (\rho_0^2 - \bar{\rho}_-^2) (\theta_-)^2 \\ & + \frac{v^2 \rho_0}{4(\rho_0^2 - \bar{\rho}_-^2)} [(\nabla \delta\rho_+)^2 + (\nabla \delta\rho_-)^2] \\ & + \frac{v^2 \bar{\rho}_-}{2} \nabla \theta_+ \cdot \nabla \theta_- - \frac{v^2 \bar{\rho}_-}{2(\rho_0^2 - \bar{\rho}_-^2)} \nabla \delta\rho_+ \cdot \nabla \delta\rho_- \end{aligned} \quad (26)$$

where the B terms leads to the mass term of θ_- , the last line is the coupling between the $+$ and $-$ mode [33]. In the absence of the Zeeman field $h = 0$, $\bar{\rho}_- = 0$, then the $+$ and $-$ modes decouple, this corresponds to the balanced BQHE.

The general expressions for the two eigen-modes are complicated. So we only list its long-wavelength limit:

$$\begin{aligned} \omega_{\text{CA}}^+(k) = & \sqrt{2\rho_0 U v^2 k^2} \\ \omega_{\text{CA}}^-(k) = & \sqrt{\Delta_R^2 + v_R^2 k^2} \end{aligned} \quad (27)$$

where $\rho_0 = \bar{\rho}_1 + \bar{\rho}_2 = -r/U$, $\theta_0 = \arccos(h/h_c)$ and

$$\begin{aligned} \Delta_R = & 2\sqrt{B/A^3}(h_c^2 - h^2), \\ v_R^2 = & 2\rho_0(A + B\rho_0 \sin^2 \theta_0)v^2 \end{aligned} \quad (28)$$

The $+$ mode is nothing but the superfluid Goldstone mode. While the $-$ mode is the roton mode whose energy takes a relativistic form with a roton gap: vanishes as $\Delta_R \sim h_c - h$ when $h \rightarrow h - h_c^-$. Obviously, it is the B term which opens the gap to the roton mode.

8. The Z-FM SF phase at $h \geq h_c$.

Above the critical point $h > h_c$, it is more convenient to introduce a mixed coordinate system with $\psi_1 = \sqrt{\rho_1 + \delta\rho_1} e^{i\theta_1}$ in the polar coordinate and ψ_2 in the Cardian coordinate. So $(\delta\rho_1, \theta_1)$ and ψ_2 are all small, the Lagrangian density becomes

$$\begin{aligned} \mathcal{L}_{\text{FM}} = & i\delta\rho_1 \partial_\tau \theta_1 + v^2 \rho_0 (\nabla \theta_1)^2 + \frac{m_1^2}{2} (\delta\rho_1)^2 + \frac{v^2}{4\rho_0} (\nabla \delta\rho_1)^2 \\ & + \psi_2^* \partial_\tau \psi_2 + v^2 |\nabla \psi_2|^2 + r_2 |\psi_2|^2 + \frac{1}{2} (U + A) |\psi_2|^4 \\ & + (U - A) \delta\rho_1 |\psi_2|^2 + B(\rho_0 + \delta\rho_1)^2 |\psi_2|^4 \\ & + \frac{B}{2} (\rho_0 + \delta\rho_1)^2 [(e^{-i\theta_1} \psi_2)^4 + (e^{i\theta_1} \psi_2^*)^4] \end{aligned} \quad (29)$$

where $m_1^2 = U + A4$ and $r_2 = r + h + (U - A)\rho_0 = 2(h - A\rho_0) = 2(h - h_c)$.

To study the universality class of the transition, it is sufficient only to keep the lowest order coupling terms:

$$\begin{aligned} \mathcal{L}_{\text{FM}} = & \psi_2^* \partial_\tau \psi_2 + v^2 |\nabla \psi_2|^2 + r_2 |\psi_2|^2 + u_2 |\psi_2|^4 \\ & + i\Gamma \delta\rho_1 \partial_\tau \theta_1 + v^2 \bar{\rho}_1 (\nabla \theta_1)^2 + \frac{1}{2} m_1^2 (\delta\rho_1)^2 \\ & + \gamma_0 \delta\rho_1 |\psi_2|^2 + \gamma_1 [e^{-i4\theta_1} \psi_2^4 + e^{i4\theta_1} \psi_2^{*4}] \end{aligned} \quad (30)$$

where we dropped $(\nabla \delta\rho_1)^2$ term which is irrelevant anyway [33], $u_2 = \frac{1}{2}(U + A + 2B\bar{\rho}_1^2)$, $\gamma_0 = U - A$, $\gamma_1 = \bar{\rho}_1^2 B/2$. $\Gamma = 1$ at the bare level, but was introduced to keep track of its flow under RG. The first line is the quantum critical mode of ψ_2 in the universality class of zero density superfluid to Mott (SF-Mott) transition, therefore has the critical exponents $z = 2, \nu = 1/2, \eta = 0$. The second line stands for the gapless SF mode of $(\delta\rho_1, \theta_1)$. The third line is the coupling between the two sectors with the coupling parameters γ_0, γ_1 .

From the quadratic parts of Eq.30, one can

extract the two eigen-modes in the long wavelength limit:

$$\begin{aligned} \omega_{\text{FM}}^+ &= \sqrt{2\rho_0(A + U)v^2 k^2} \\ \omega_{\text{FM}}^- &= 2(h - h_c) + v^2 k^2 \end{aligned} \quad (31)$$

which has the dynamic exponent $z = 2$.

Contrasting Eq.27 with Eq.31, one can see that due to the extra A term in the latter, the SF velocity increases from $h \ll h_c$ to $h \gg h_c$, while the difference $(v_{\text{FM}}^+)^2 - (v_{\text{CA}}^+)^2 = 2\rho_0 A v^2 k^2$ maybe a good measure of the A term. However, the SF density $\rho_s = \rho_0 v^2$ remains the same as shown in Fig.1b. The roton $-$ mode's gap vanishes as $\Delta_R \sim |h - h_c|$ on both sides, However, the roton gap at $h > h_c$ seems independent of the B term, while that at $h < h_c$ is a good measure of the B term.

9. The nature of the quantum critical point at $h = h_c$ and new dangerously marginally irrelevant operators

By keeping both SF $(\delta\rho_1, \theta_1)$ mode and the critical ψ_2 mode in Eq.30, one can perform RG flow on the two couplings γ_0, γ_1 between the two sectors.

The RG analysis can be done by following the procedures developed in [35] which study the SF to metal transition in a high temperature superconductor. The first line in Eq.30 stands for the critical mode with the dynamic exponent $z = 2$, one can scaling dimension of the critical field $[\psi_2(\vec{x}, \tau)] = 1$, then $[u_2] = 0$ is marginally irrelevant at the upper critical dimension $d_u = 2$. The second line stands for the SF mode with its own dynamic exponent $z_{\text{SF}} = 1$. This is contrast to the case in [35] where both the boson and the fermion have the same dynamic exponent $z = 2$. However, to be consistent with the ψ_1 mode, one must still choose $z = 1$. Then one can determine the scaling dimensions of the magnitude fluctuation $[\delta\rho_1(\vec{x}, \tau)] = 2$, and the phase mode $[\theta_1(\vec{k}, \omega)] = -3$. Then the Berry phase term $[\Gamma] = -1$, so it becomes irrelevant, then the magnitude fluctuation $\delta\rho_1$ and the phase mode are asymptotically decoupled. Similar phenomena happens in the two channel Kondo model [36] where the Berry term also becomes irrelevant and turns into a boundary condition for the Majorana fermions! The third line which stands for the coupling between the two sectors, so can determine $[\gamma_0] = 0$, so it is marginal. Similar, one can also determine $[\gamma_1] = 0$, so it is also marginal.

1. The effective action

To construct an effective action to study the nature of the QCP, one can simply integrate out $(\delta\rho_1, \theta_1)$ in Eq.30 to study how the SF phase fluctuation affect the quantum critical behaviors of the ψ_2 mode. Because the $\delta\rho_1$ is always massive with the mass m_1 , so can be integrated out to generate a $|\psi_2|^4$ term, so can be absorbed into the coefficient u_2 . One can also see $\langle e^{-i4\theta_1} \rangle = \langle e^{i4\theta_1} \rangle = e^{-8\langle \theta_1^2 \rangle}$ is a finite constant at $d = 2 + 1$ dimension which stands for the suppression of the BEC condensate at $T = 0$. So integrating out $(\delta\rho_1, \theta_1)$ leads to the effective action describing the transition driven by the roton dropping:

$$\begin{aligned} \mathcal{L}_{\text{QC}} = & \psi_2^* \partial_\tau \psi_2 + v^2 |\nabla \psi_2|^2 + r_2 |\psi_2|^2 + u_2 |\psi_2|^4 \\ & + \gamma_1 [\psi_2^4 + \psi_2^{*4}] + \dots \end{aligned} \quad (32)$$

where only the last term breaks the $U(1)$ symmetry to the underlying $[C_4 \times C_4]_D$ symmetry. However, it can be shown this symmetry breaking γ_1 term is marginally irrelevant at the $z = 2, \nu = 1/2, \eta = 0$ universality class at $d = 2$. But it is still dangerously irrelevant at $h < h_c$, leads to the CAFM state in Fig.3a.

If the Berry phase term in Eq.32 had become a second derivative $|\partial_\tau \psi_2|^2$, then the dynamic exponent would be $z = 1$, then it is in the 3d XY universality class. Then the γ_1 maybe shown to be irrelevant near this 3d XY QCP by

$\epsilon = 3 - d$ expansion [16]. But here it is a Gaussian fixed point with $z = 2$, we expect it is marginally irrelevant. Because both u_2 and γ_1 are marginally irrelevant, doing RG calculations, one must treat u_2 and γ_1 on the same footing. Because the γ_1 term breaks the $U(1)$ symmetry, it may lead to logarithmic corrections [16] different from those just due to the u_2 term shown in Eq.34.

In Eq.32, at $r_2 < 0$, ψ_2 has a condensation $\psi_2 = \sqrt{\rho_2 + \delta\rho_2}e^{i\theta_2}$, then to quadratic order, the Lagrangian becomes

$$\mathcal{L}_R = i\delta\rho_2\partial_\tau\theta_2 + v^2\left[\frac{1}{4\bar{\rho}_2}(\nabla\delta\rho_2)^2 + \bar{\rho}_2(\nabla\theta_2)^2\right] + u_2(\delta\rho_2)^2 + 16\gamma_1\bar{\rho}_2^2(\theta_2)^2 \quad (33)$$

where we have set the linear term $(r_2 + 2u_2\bar{\rho}_2)\delta\rho_2$ vanishing to find $\bar{\rho}_2 = -r_2/(2u_2)$. Then one can extract the eigen mode $\omega_R = \sqrt{(v^2k^2 + 4\bar{\rho}_2u_2)(v^2k^2 + 16\gamma_1\bar{\rho}_2)} \approx \sqrt{64\gamma_1\bar{\rho}_2^2u_2 + \bar{\rho}_2(4u_2 + 16\gamma_1)v^2k^2}$ which recovers the ω_- mode in Eq.27. Note that it is the γ_1 term which leads to the mass of the phase θ_2 .

2. Quantum critical scalings and quantum information scramblings in the QC regime near h_c .

The order parameter is the magnetization in the XY plane $\langle S^x \rangle$. It vanishes in the Z-FM SF phase, but non-zero in the CAFM SF phase. Because the γ_1 term breaks the $U(1)$ symmetry, but is marginally irrelevant at $d = 2$. There is an emergent $U(1)$ symmetry at the QCP which indicates the CAFM SF to the Z-FM SF transition is in the same universality class of the zero-density SF-mott transition with the critical exponents $z = 2, \nu = 1/2, \eta = 0$ studied in Ref.[15]. However, the two phases are very much different from the SF and Mott. In the CAFM SF, there is $\cos 4\phi$ clock term in Eq.18 which is dangerously irrelevant near the QCP: it is irrelevant near the QCP, but controls the quantum phase $h < h_c$. It leads to the CAFM SF phase, breaks the presumably $U(1)$ symmetry to the joint C_4 symmetry and also opens a gap Eq.27 to the roton mode. There is a melting transition T_M above the CAFM SF phase (Fig.1b). The universality class of melting process belongs to 2D $q = 4$ state clock transition.

The standard scaling shows the roton gap should scale as $\Delta_R \sim |h - h_c|^{z\nu} \sim |h - h_c|$ which is consistent with our specific calculations shown above. The specific heat should scale as $C_R \sim T^{d/z} \sim T$. Our specific calculations show that the specific heat due to the roton in the spin sector is $C_R = \frac{\pi^3}{3v^2}T$. Applying the scaling result for the $U(1)$ conserved quantity in [15] to the order parameter leads to :

$$\left\langle \frac{1}{N_s} \sum_i [(S_i^x)^2 + (S_i^y)^2] \right\rangle = \frac{2mT}{4\pi} \frac{1}{\{\ln[\Lambda^2/(2mT)]\}^4} \quad (34)$$

where $m = 1/(2v^2) = t_0/(2t_0^2 - t_{so}^2)$ and Λ is a momentum upper cutoff [16].

Obviously, due to the non-linearities in Eq.21 and 32, the system shows quantum chaos [18–20] in the QC regime. The quantum information scrambling encoded in the spinor boson out of time ordered correlation function (OTOC):

$$\langle \psi_\alpha^\dagger(t, \vec{x}) \psi_\alpha^\dagger(0, 0) \psi_\alpha(t, \vec{x}) \psi_\alpha(0, 0) \rangle \sim e^{\lambda_{L,\alpha}(t-x/v_{B,\alpha})}, \quad (35)$$

where $\alpha = 1, 2$ stand for SF component and Roton component in Eq.19 respectively. Near the lightcone $x = v_{B,\alpha}t$ (Fig.5), the OTOC is greatly enhanced in the QC regime in Fig.1. The Lyapunov exponent $\lambda_{L,\alpha}$ due to the critical roton mode reaches its maximal value $\lambda_{L,R} \sim T$, while the butterfly velocity $v_{B,R} \sim T^{1-1/z}$. For $z = 2$, $v_{B,R} \sim \sqrt{T}$. From the dimensional analysis [37], we conclude $v_{B,R} \sim v\sqrt{T}$ [16].

Note that the SF sector stays un-critical across the QCP. We obtain the finite KT transition temperature (Fig.1b) $T_{KT} = \frac{\pi}{2}\rho_s \sim \pi n_0 v^2$. The Lyapunov exponent due to the SF mode [21] is $\lambda_{L,sf} \sim T^3/\rho_s^2$ and its butterfly velocity $v_{B,sf} \sim c = v\sqrt{2n_0U}$ as can be seen from Eq.27,31.

From Eq.21, using Eq.20 and shifting the orders of the operators in Eq.35, one may also evaluate the transverse spin-spin correlation function, $\langle S^+(t, \vec{x}) S^-(0, 0) \rangle = (-1)^{i-j} \langle \psi_1^\dagger(t, \vec{x}) \psi_2(t, \vec{x}) \psi_2^\dagger(0, 0) \psi_1(0, 0) \rangle$. Note that it can only be evaluated from the original action Eq.21 instead of the effective action Eq.32 where the SF model ψ_1 has been integrated out.

10. Contrast the GL approach with the microscopic calculations in studying the NOFQD phenomena

The two approaches are completely independent and complementary to each other. Both have its own advantages and limitations. It is very constructive to contrast phenomenological approach in Sec.5-8 with the microscopic calculations in Sec.2-4. We can see the following mappings between the parameters in the phenomenological GL action Eq.21 which holds at any h and those evaluated by the microscopic calculations at $h = 0$ in Sec.5 and Sec.B in the SM, especially the effective potential generated by the OFQD:

$$v^2 = (t_0^2 - t_{so}^2/2)/t_0, \quad r = -(\mu + 4t) \\ A = A_m n^2, \quad B = B_m n^4, \quad (36)$$

where the subscript m indicates the parameters evaluated by the microscopic calculations at $h = 0$ in Sec.2-5.

The interaction U and the Zeeman field h are the same in both approaches. Especially, it indicates that the A and B in the GL action are nothing but the effective potential generated by OFQD upto a density dependence. So both are positive at $h = 0$ in the weak coupling limit. However, their signs may change as the interaction increases from the weak to strong couplings [31].

From Eq.31, one can see the roton spectrum matches that achieved by microscopic calculation at its valid

regime: high h limit. For example, the gap $\Delta_R = 2(h - h_c)$ matches the microscopic calculations in the high h limit in Sec.2. This fact may also be related to the mapping shown in the first row of Eq.36 that the GL parameter r in Eq.21 is pinned at $r = -\rho_0 U$ when $h \leq h_c$, but increases linearly $r = (h - h_c) - \rho_0 U$ matches the chemical potential $-(\mu + 4t) = h - n_0 U$ in the microscopic calculations in Sec.2.

The density dependence of A and B in Eq.36 is important in the evaluations of excitation spectrum at $h > h_c$ and $h < h_c$, especially the nature of the QCP. Had one ignored the quantum fluctuations in the density channel (for example, by fixing it to be the BEC condensate $n = n_0$), one would have found the Zeeman field only couples to the spin sector, therefore leads to the un-physical physical picture: the SF sector is completely decoupled from the spin sector. Of course, A and B also depend on h , so the mapping Eq.36 only holds at $h = 0$.

Most importantly, for the very first time, we establish the connections between the GL action and the OFQD evaluated by microscopic calculations ! This observation also endows the physical meaning of the OFQD from a complete new and deep perspective.

11. Analogy and difference from the bilayer quantum Hall effects at the total filling factor $\nu_T = 1$.

It is very instructive to compare the Bilayer quantum Hall effects (BLQH) [28–30] at the total filling factor $\nu_T = 1$: Eq.21 is similar to the effective Chern-Simon Ginsburg-Landau (CSGL) composite boson theory of the BLQH: in the absence of B term, the symmetry is $U(1)_1 \times U(1)_2 = U(1)_+ \times U(1)_-$, while the B term breaks the $U(1)_-$ symmetry and opens a gap to the putative Goldstone mode and transfers it into a pseudo-Goldstone mode. The U term maps to the intra-layer Coulomb interaction, the A term maps to the inter-layer capacitive term at a finite distance d . However, there are also several crucial differences: (1) Here, both $+$ and $-$ sector are charge neutral. While in BLQH, only $-$ is the charge neutral, there is a Chern-Simon term in the $+$ charge sector which opens a charge gap to the putative SF Goldstone mode, leads to the QH with the quantized Hall conductivity $\sigma_H = 1$ in the charge sector and the topological charges of the merons. (2) Here, as shown in Eq.36 at the microscopic level, the A term and B term are the effective potentials generated by OFQD in Eq.15 which depend on the t/U . However, in BLQH, the capacitive A term is due to the difference between intra- and inter-layers Coulomb interactions tunable by the distance d of the two layers. The B term is similar to the inter-layer tunneling term $H_t = -t(\psi_1^* \psi_2 + h.c)$ which can also be manipulated by the in-plane magnetic field. (3) Here the " tunneling term " between the two species ψ_1, ψ_2 is the 4th power dictated by the underlying $[C_4 \times C_4]_D$ symmetry. However, it is just 1st power in BLQH. The power difference in the interlayer tunneling

makes dramatic differences in the two systems. Here, the 4th power was shown to be marginally and dangerously irrelevant near the QCP in Fig.1a, but opens the gap to the roton mode. However, the 1st power was known to be relevant in BLQH., opens a gap to the interlayer SF Goldstone mode, essentially destroys the interlayer phase coherence. (4) Here, there is a roton dropping transition tuned by the Zeeman field h when either ψ_1 or ψ_2 is depleted and the spin is polarized along the z direction in Fig.1a. In principle, in the absence of the inter-layer tunneling term H_t , the $\nu_T = 1$ BLQH is independent of the bilayer imbalance, there is always a neutral gapless mode. As the distance d increases, there maybe a roton dropping transition in the charge neutral sector leading to a first order transition from the exciton superfluid (ESF) to pseudo-spin density wave (PSDW)[28–30]. Both the roton mode at a finite wavevector $|\vec{k}| = k_0$ and SF mode near the zero wavevector $\vec{k} = 0$ happen in the $-$ mode, the origin of the roton mode is due to the inter-layer interaction, so very much different from the roton mode here tuned by the Zeeman field in Fig.3. The main difference is that the BLQH is in a continuous system, so the roton is at a 1d roton ring driving a 1st order transition, while here is on a square lattice, so the roton is at (π, π) driving a 2nd order transition. (5) Here, we did the microscopic calculations by the Bogoliubov calculations at any Zeeman field h which can be contrasted with the phenomenological GL action Eq.21. While, in the BLQH, there is a also a microscopic calculation called Hartree-Fock (HF) projected within the Lowest Landau level (LLL) which was also compared to the phenomenological Chern-Simon GL effective action [30].

12. Detectable experimental implications in cold atoms.

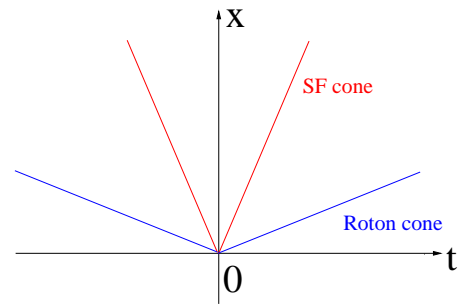


FIG. 5. In the quantum information scrambling characterized by the OTOC Eq.35 near $h = h_c$, there is a wide separation between the SF cone $x_{sf} = v_{B,sf}t$ for $\alpha = 1$ and the roton cone $x_B = v_{B,R}t$ with $v_{B,sf} \gg v_{B,R}$ for $\alpha = 2$.

In the ongoing experiment [7], the BEC has $N \sim 3 \times 10^5$ atoms and trapped within the diameter $d = 80 \mu\text{m}$, so one lattice site has about $n = 10$ atoms. For typical experiment parameters, optical lattice potential is $4.16 E_r$, and Raman potential is $1.32 E_r$, where $E_r = 375$ nK de-

notes the recoil energy, so the tight binding model parameter can be estimated as $t_0 \sim 100$ nK, $t_{so} \sim 30$ nK, so $t_{so}/t_0 \sim 1/3$. The short-range Hubbard like interaction $U = \frac{4\pi\hbar^2 a_s}{m} \int d^2r |w(r)|^4$, where s -wave scattering length of the ^{87}Rb atoms $a_s = 103a_0$ and a_0 is the Bohr radius and the mass of the bosons ^{87}Rb lead to $U \sim 10$ nK, so $n_0 U \sim 100$ nK.

Based on these experimental parameters, one can estimate $T_{KT} \sim 100$ nK, the roton gap away from the critical point in Fig.3b $\Delta_R \sim 1$ nK, so the melting transition $T_M \sim 1$ nK and the critical Zeeman field $h_c \sim 1$ mG. So far, the experiments are operating at $T \sim 20$ nK. As noted earlier, there is also a specific heat contribution from the superfluid sector $C_{sf} = \frac{\pi}{n_0 U v^2} T^2 \sim (T/n_0 U) T/v^2 \ll T/v^2 \sim C_R$ which is sub-leading to that from the critical roton mode in the spin sector. Of course, the SF sector makes no contributions to the magnetization Eq.34. In terms of quantum information scramblings, the Lyapunov exponent due to the SF mode $\lambda_{L,sf} \sim T^3/\rho_s^2 \sim T(T/\rho_s)^2 \sim T(T/T_{KT})^2 \ll T \sim \lambda_{L,R}$, while its butterfly velocity $v_{B,sf} \sim c = v\sqrt{2n_0 U} \gg v_{B,R} = v\sqrt{T}$. This means the light cone of the SF mode $x_{sf} = v_{B,sf}t$ is well within that of the roton mode $x_R = v_{B,R}t$ (Fig.5). Due to the wide separation of the two light-cones, both light-cones could be detected in the spinor boson (see Eq.19), spin or density OTOC. So we conclude that the current experimental operating temperatures may not be able to get into the CAFM SF phase, but are still low enough such that the dramatically quantum critical fluctuation effects in the specific heat, Lyapunov exponent, butterfly velocity, transverse magnetization, boson or spin correlation functions can be detected by dynamic or elastic, energy or momentum resolved, longitudinal or transverse Bragg spectroscopies [22–24], specific heat measurements [25, 26] and in-situ measurements [27].

13. Conclusions and discussions

In this work, we propose a new concept: NOFQD. We also perform both microscopic and effective GL action to implement this new concept in the specific QAH Hamiltonian Eq.1. We did microscopic calculations at both weak and strong couplings at both $h = 0$ and $h \gg U$. Then we construct the effective GL action at any h and contrast with the microscopic calculations at both $h = 0$ and very strong Zeeman field $h \gg U$. However, only the GL action can capture the competition near $h \sim h_c$.

In order to clarify the connections and relations between the conventional OFQD and the NOFQD studied here, according to its response to a given deformation which breaks either an exact symmetry or a spurious symmetry or both, we classify OFQD into two classes:

1. Type-I OFQD response trivially to a deformation:

In type-I, at a high symmetry point, there is an exact symmetry and also a spurious continuous symmetry, the OFQD breaks the spurious symmetry down to the exact symmetry and selects the quantum ground state upto the

exact symmetry. Then a deformation λ away from the high symmetric point breaks the exact symmetry explicitly, but may or may not break the spurious symmetry, it just pick up a state from the exact degenerate manifold. If the spurious symmetry remains at $\lambda \neq 0$, then the OFQD analysis at $\lambda \neq 0$ is very similar to that at $\lambda = 0$ (Fig.6a).

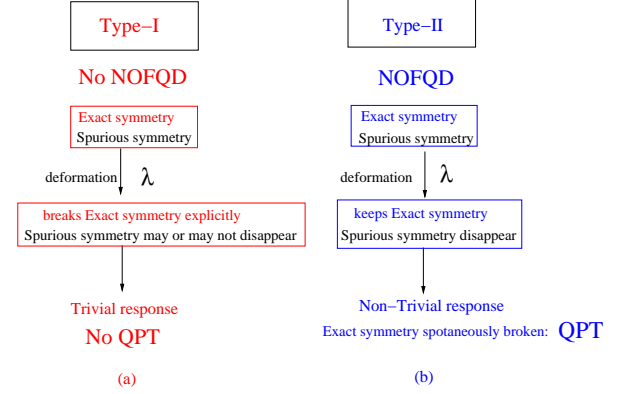


FIG. 6. Contrast Type-I in (a) with type-II OFQD in (b) which response trivially and non-trivially to a deformation respectively. Shown are relations among the deformation, exact symmetry and spurious symmetry and their explicitly broken by the deformation λ or spontaneously broken through a QPT. The QPT in Type-II happens when λ matches the energy scale of the effective potential generated by the OFQD at $\lambda = 0$.

2. Type-II OFQD response non-trivially to a deformation and leads to NOFQD

In type-II, at a high symmetry point, there is an exact symmetry and also a spurious continuous symmetry. The OFQD breaks the spurious symmetry down to the exact symmetry and selects the quantum ground states upto the exact symmetry. Then a deformation λ away from the high symmetric point keeps the exact symmetry, but breaks the spurious symmetry. There is a competition between the effective potential generated by the OFQD at $\lambda = 0$ and the deformation λ as λ evolves, which drives a QPT due to the spontaneously symmetry breaking of the exact symmetry. The QPT happens when λ matches the scale of the effective potential. This is what we called NOFQD: despite there is no spurious symmetry anymore when $\lambda \neq 0$, but the effective potential generated at $\lambda = 0$ still has a dramatic effect when $\lambda \neq 0$ (Fig.6b).

It maybe constructive to compare this classification with that of superconductors in the response to an orbital magnetic field: in Type-I, there is a direct transition from the normal state to a superconducting state at just one critical field h_c , in Type-II, there is a mixed state intervening between the low h_{c1} and high critical field h_{c2} .

3. Two examples of Type I OFQD under SOC

In a recent work on complete/In-complete devil stair cases in the strong coupling limit of SOC [17], there is

an exact $[C_4 \times C_4]_D$ symmetry and also a spurious $U(1)$ symmetry, along the diagonal line $\alpha = \beta$ near the Abelian point $\alpha = \beta$ in the SOC parameter space. The OFQD analysis selects either Y-x or X-y state as the quantum ground state which rotates to each other under the exact $[C_4 \times C_4]_D$ symmetry. However, slightly away from the diagonal line $\alpha \neq \beta$, then it breaks the exact $[C_4 \times C_4]_D$ symmetry explicitly, the spurious $U(1)$ symmetry also disappears. Then a simple classical analysis picks up Y-x or X-y state when $\alpha > \beta$ or $\alpha < \beta$ respectively. Therefore, the OFQD at $\alpha = \beta$ response trivially to the deformation $\alpha \neq \beta$.

For another example, for the $(\alpha = \pi/2, \beta)$ SOC case which has an exact $U(1)_{soc}$ symmetry at the spin anisotropic interaction $\lambda = 1$. There is also a spurious $U(1)$ symmetry at $\lambda = 1$. At $\lambda = 1$, the OFQD at the weak coupling selects the PW-X phase upto the exact $U(1)_{soc}$ symmetry to be the quantum ground state. For example, the Z-x phase and the PW-X transform to each other under the exact $U(1)_{soc}$ symmetry. When $\lambda < 1$, it explicitly breaks the exact $U(1)_{soc}$ symmetry, but the spurious $U(1)$ symmetry remains, then a similar OFQD analysis selects the PW-X phase to be the quantum ground state. When $\lambda > 1$, it also explicitly breaks the exact $U(1)_{soc}$ symmetry, the spurious $U(1)$ symmetry also disappears, then a simple classical analysis alone picks up the Z-x state to be the ground state. So the OFQD at $\lambda = 1$ response trivially to the deformation $\lambda \neq 1$.

Both examples belong to Type-I, the deformation breaks the exact symmetry at the high symmetric point, but it may or may not break the spurious symmetry. There is NO competition between the effective potential generated by the OFQD at the high symmetric point and the deformation away from the high symmetric point, no associated QPT either, therefore no NOFQD phenomena.

4. Two examples of Type II OFQD under SOC

For the QAH studied in this work, at $h = 0$, it has the \mathcal{M} symmetry and the exact $[C_4 \times C_4]_D$ symmetry. At $h = 0$ there is also a spurious $SU(2)_s$ symmetry, an OFQD analysis selects the $N = 2$ XY-AFM SF as the quantum ground state and also opens a gap to the roton mode. This state has the $d = 4$ degeneracy, keeps the \mathcal{M} symmetry, but breaks the exact $[C_4 \times C_4]_D \rightarrow 1$ symmetry spontaneously. Any small $h \neq 0$ breaks the \mathcal{M} symmetry, but still keeps the exact $[C_4 \times C_4]_D$ symmetry. The spurious $SU(2)_s$ symmetry disappears, a simple classical analysis picks up the Z-FM SF which keeps the exact $[C_4 \times C_4]_D$ symmetry. Then there is an associated QPT from the $N = 2$ XY-AFM SF state to the Z-FM as h increases (Fig.1). The exact $[C_4 \times C_4]_D$ symmetry was spontaneously broken in the $N = 2$ XY-AFM SF state, but restored in the Z-FM state. Of course, one need to check if the 2nd QPT be pre-empted by other competing phases. By both microscopic and effective GL action, we show that this does not happen. Despite there are

many known examples of TYPE-I, we expect Type-II is also transformative to many other systems. For example, in a recent unpublished work [38], we show that Type-II also appears in the interacting bosonic Haldane model in a honeycomb lattice subject to a sublattice potential.

4. Contrast to $NAdS_2/NCFT_1$ in SYK models

It is very instructive to compare the NOFQD with the $NAdS_2/NCFT_1$ correspondence in the SYK model. In the latter, one must move slightly away from the 1d CFT to take into accounts the leading irrelevant operator $-i\omega$ to study the OTOC and extract its quantum Lyapunov exponent. Here, a small h is also slightly away from $h = 0$ where the OFQD selects a quantum ground state such as the $N = 2$ XY-AFM SF state. In the RG sense, due to the small roton gap, a small h is also irrelevant. However, the main difference is that in the SYK models, the ground state is a gapless QSL state which breaks the 1d CFT (reparametrization) invariance spontaneously to $SL(2, R)$ leading to a zero (Goldstone) mode, the irrelevant deformation $-i\omega$ breaks the 1d CFT (reparametrization) invariance explicitly, lifts the zero mode to a pseudo-Goldstone mode leading to maximal chaos, but does not drive any QPT. While here the $N = 2$ XY-AFM SF state breaks the exact $[C_4 \times C_4]_D$ symmetry spontaneously and has a roton gap, the Zeeman field h keeps the exact $[C_4 \times C_4]_D$ symmetry, it reduces the roton gap and just tilts the $N = 2$ XY-AFM state into the CAFM state which has the same symmetry as the $N = 2$ XY-AFM SF state. However, a sufficiently large h does drive a transition to the Z-FM SF. Of course, $NAdS_2/NCFT_1$ correspondence is only for 1d, at higher dimension such as $NAdS_{d+1}/NCFT_d$ with $d \geq 2$, there is no need to move slightly away from CFT, so nearly is not necessary. Here, although we demonstrate it in only 2+1 dimension, the NOFQD happens in any dimension.

As stressed in Sec.5, the original goal of constructing the GL action is to study the transition from weak coupling to strong coupling at an integer filling. Here, we use it to investigate the transition driven by the Zeeman field h within the weak coupling regime, so the system remains inside a SF phase. We leave our original goal to a future work [31]. In a future work, directly inspired by the experimental realizations, we look at the deformation due to $t_{sx} \neq t_{sy}$ which breaks the exact $[C_4 \times C_4]_D$ symmetry explicitly to $[C_2 \times C_2]_D$. We will do microscopic calculations at both weak and strong couplings.

Acknowledgements

We thank Bao-Zong Wang and Zhan Wu for helpful discussions on experimental detections. We also thank B. Halperin for the critical discussions in [13] and some other helpful comments on the manuscript. We acknowledge AFOSR FA9550-16-1-0412 for supports.

-
- [1] M. Z. Hasan and C. L. Kane, Colloquium: Topological insulators, *Rev. Mod. Phys.* **82**, 3045 (2010).
- [2] X. L. Qi and S. C. Zhang, Topological insulators and superconductors, *Rev. Mod. Phys.* **83**, 1057 (2011).
- [3] Rui Yu, Wei Zhang, Hai-Jun Zhang, Shou-Cheng Zhang, Xi Dai1, Zhong Fang, Quantized Anomalous Hall Effect in Magnetic Topological Insulators, *Science* **329**, 61 (2010).
- [4] Cui-Zu Chang, Jinsong Zhang, Xiao Feng, Jie Shen, Zuocheng Zhang, Minghua Guo1, Kang Li, Yunbo Ou, Pang Wei, Li-Li Wang, Zhong-Qing Ji, Yang Feng1, Shuai-hua Ji, Xi Chen, Jinfeng Jia1, Xi Dai2, Zhong Fang2, Shou-Cheng Zhang3, Ke He2,?, Yayu Wang1,?, Li Lu2, Xu-Cun Ma2, Qi-Kun Xue1, Experimental Observation of the Quantum Anomalous Hall Effect in a Magnetic Topological Insulator, *Science* **340**, 167 (2013).
- [5] Lianghui Huang, *et.al*, Experimental realization of a two-dimensional synthetic spin-orbit coupling in ultracold Fermi gases, *Nature Physics* **12**, 540-544 (2016).
- [6] Zengming Meng, *et.al*, Experimental observation of topological band gap opening in ultracold Fermi gases with two-dimensional spin-orbit coupling, *arXiv:1511.08492*.
- [7] Zhan Wu, Long Zhang, Wei Sun, Xiao-Tian Xu, Bao-Zong Wang, Si-Cong Ji, Youjin Deng, Shuai Chen, Xiong-Jun Liu, Jian-Wei Pan, Realization of two-Dimensional spin-orbit coupling for Bose-Einstein condensates, *Science* **354**, 83 (2016).
- [8] The end of the boundary sits at the origin $t_{so} = 0, h = 0$ which has the exact $SU(2)$ symmetry, the other parts only have the emergent $U(1)$ symmetry. The whole line has the dynamic exponent $z = 2$. As demonstrated in the text, it has the same universality class as the zero density SF-Mott transition subject to a new marginally and dangerously irrelevant anisotropic term.
- [9] Fadi Sun, Junsen Wang, Jinwu Ye and Youjin Deng, Symmetry protected bosonic topological phase transitions: Quantum Anomalous Hall system of weakly interacting spinor bosons in a square lattice, *arXiv:1711.11580*, substantially revised version as version 2.
- [10] This is because there are 2 valleys in Eq.9, 2 spins and the particle-hole spaces leading to the 8×8 Bogoliubov transformation and the Reduced BZ in Eq.10.
- [11] D. van Oosten, P. van der Straten, and H. T. C. Stoof, Quantum phases in an optical lattice, *Phys. Rev. A* **63**, 053601 (2001).
- [12] See the supplementary materials for more details to establish the effective potential Eq.14 and 15 generated by the order from quantum disorder. The analytical approach is based on a perturbation theory in t_{so}/t_0 , and the numerical approach is a direct numerical evaluation which confirms the analytical calculations on $\omega_{l,k}$ and $E_{ofd}(\theta, \phi)$ defined in Eq.4.
- [13] We thank B. Halperin for alerting us this fact which inspired us to discover the nearly order from quantum disorder (NOFQD) phenomena and the associated quantum phase transition, then develop both the microscopic and phenomenological approaches to study the NOFQD phenomena.
- [14] Subir Sachdev, *Quantum Phase Transitions*, 2nd ed. (Cambridge University Press, Cambridge, 2011).
- [15] Subir Sachdev, T. Senthil, and R. Shankar, Finite-temperature properties of quantum antiferromagnets in a uniform magnetic field in one and two dimensions, *Phys. Rev. B* **50**, 258 (1994).
- [16] For notational simplicity, dropping the subscript 2 and writing ψ in terms of its real and imaginary part $\psi = \phi_1 + i\phi_2$, then the interaction terms in Eq.32 can be written as $(u - 6\gamma)(\phi_1^2 + \phi_2^2)^2 + 8\gamma(\phi_1^4 + \phi_2^4)$ where the second term is the cubic anisotropic term with $N = 2$ real components. Its RG flow at $\epsilon = 3 - d > 0$ was well known at any N component with 4 RG fixed points (1) Gaussian fixed point $u^* = v^* = 0$ (2) Ising fixed point $u^* = 0, v^* > 0$ (3) $O(N)$ fixed point $u^* > 0, v^* = 0$ and (4) Cubic fixed point $u^* > 0, v^* \sim (N - 4)\epsilon \neq 0$. The fixed point structure changes from $N > 4$ where the cubic fixed point $u^* > 0, v^* > 0$ is the only stable fixed point to $N < 4$ where the $O(N)$ fixed point is the only stable fixed point. So when $N = 2 < 4$, it belongs to the latter case where the cubic anisotropy is irrelevant near the 3d XY fixed point. At the upper critical dimension $\epsilon = 0$, all the 4 fixed points converge to the Gaussian fixed point. It is interesting to repeat this calculation at $d = 2, z = 2$ where the upper critical dimension $d = 2$ and $\epsilon = 0$. For example, we will put u_2 and γ_1 in Eq.32 at the same footing to perform the RG analysis, also evaluate the new logarithmic corrections to Eq.34 due to the two marginally irrelevant couplings. In fact, just like the transverse magnetization in Eq.34, the specific heat C_R , the Lyapunov exponent λ_L , the butterfly velocity $v_{B,R}$ will all receive a logarithmic factor at a finite T .
- [17] Fadi Sun and Jinwu Ye, Fractals, complete and incomplete devil staircases of strongly interacting spin-orbit coupled bosons in a lattice, *arXiv:1603.00451*, substantially revised version.
- [18] S. Sachdev and J. Ye, Gapless spin liquid ground state in a random quantum Heisenberg magnet, *Phys. Rev. Lett.* **70**, 3339 (1993).
- [19] A. Y. Kitaev, Talks at KITP, University of California, Santa Barbara, "Entanglement in Strongly- Correlated Quantum Matter (2015).
- [20] Fadi Sun and Jinwu Ye, Periodic Table of SYK and supersymmetric SYK, *Phys. Rev. Lett.* **124**, 244101 (2020).
- [21] Debanjan Chowdhury, Brian Swingle, Onset of many-body chaos in the $O(N)$ model, *Phys. Rev. D* **96**, 065005 (2017).
- [22] Si-Cong Ji, Long Zhang, Xiao-Tian Xu, Zhan Wu, Youjin Deng, Shuai Chen, and Jian-Wei Pan, Softening of Roton and Phonon Modes in Bose-Einstein Condensate with Spin-Orbit Coupling, *Phys. Rev. Lett.* **114**, 105301 (2015).
- [23] Jinwu Ye, J.M. Zhang, W.M. Liu, K.Y. Zhang, Yan Li, W.P. Zhang, Light scattering detection of various quantum phases of ultracold atoms in optical lattices, *Phys. Rev. A* **83**, 051604 (R) (2011).
- [24] Jinwu Ye, K.Y. Zhang, Yan Li, Yan Chen and W.P. Zhang, Optical Bragg, atom Bragg and cavity QED detections of quantum phases and excitation spectra of ultracold atoms in bipartite and frustrated optical lattices, *Ann. Phys.* **328** (2013), 103-138.
- [25] Kinast, J. *et al.* Heat Capacity of a Strongly Interacting Fermi Gas. *Science* **307**, 1296 (2005).
- [26] Ku, M. J. H. *et al.* Revealing the Superfluid Lambda Transition in the Universal Thermodynamics of a Unitary Fermi Gas. *Science* **335**, 563 (2012).
- [27] Gemelke, N., Zhang X., Huang C. L., and Chin, C. In situ observation of incompressible Mott-insulating domains in ultracold atomic gases, *Nature* (London) **460**, 995 (2009).

- [28] Jinwu Ye, Fractional charges and quantum phase transitions in imbalanced bilayer quantum Hall systems, *Phys. Rev. Lett.* 97, 236803 (2006).
- [29] Jinwu Ye and Longhua Jiang, Excitonic superfluid to pseudo-spin density wave transition in bilayer quantum Hall systems, *Phys. Rev. Lett.* 98, 236802 (2007).
- [30] Jinwu Ye, Mutual Composite Fermion and Composite Boson approaches to balanced and im-balanced bilayer quantum Hall systems: an electronic analogy of Helium 4 system, *Annals of Physics*, 323 (2008), 580-630.
- [31] Fadi Sun and Jinwu Ye, Strong coupling limit of the bosonic quantum anomalous Hall, quantum compass model in a transverse field and weak coupling to strong coupling transition, preprint in preparation.
- [32] More straightforwardly and intuitively, just like in BLQH [30], one can write the interaction term as $\frac{U}{2}[|\psi_1|^2 + |\psi_2|^2 - \rho_0]^2$ where ρ_0 is the average total atom density (or electron density in BLQH). Expanding it out automatically leads to $r = -\rho_0 U$.
- [33] In the BLQH [28–30], the two terms in the gradient of $\delta\rho_+$ and $\delta\rho_-$ were dropped due to their subleading to the corresponding mass terms.
- [34] In the absence of Zeeman field $h = 0$, the \pm modes in Eq.26 are decoupled, so the \pm mode stand for the gapless SF mode and gapped roton mode in \pm channels respectively. However, when $h > 0$, there is a mixing between the two channels whci lead to two new eigen-modes which are neither $+$ or $-$ mode. But we still use the same symbols.
- [35] J. Ye and S. Sachdev, Superconducting, metallic, and insulating phases in a model of CuO_2 layers, *Phys.Rev.B* 44, 10173 (1991).
- [36] Jinwu Ye, *Abelian Bosonization approach to quantum impurity problems*, *Phys. Rev. Lett.* 79, 1385 (1997).
- [37] In the whole manuscript, we take the lattice constant $a = 1$, so ka and x/a are dimensionless, then the butterfly velocity v_B carry the dimension of energy.
- [38] Fadi Sun *et.al* , NOFQD in bosonic Haldane model under a sublattice potential and its experimental observation, unpublished.

Supplementary Materials for “Nearly order from quantum disorder phenomena: its application and detection in the bosonic quantum anomalous Hall system”

In the main text, we present an NOFQD analysis on the weakly coupling bosonic Quantum Anomalous Hall model leading to the phase diagram in Fig.M1b. In this Supplementary Materials (SM), in the first section, we present a traditional approach which ignores the NOFQD phenomena and leads to a first order transition at $h = 0$. The breakdown of this traditional approach at $h \lesssim U$ was used to motivate the importance of the NOFQD phenomena and also inspire us to develop the new symmetry based GL approach in the main text to study the NOFQD phenomena in the most systematic and complete way. In section two, we provide the explicit form of the effective potential Eq.M15 generated by the OFQD analysis at $h = 0$ which was also predicted by the independent symmetry based GL approach.

A. THE CONVENTIONAL APPROACH WHICH IGNORES THE NOFQD PHENOMENA LEADS TO A FIRST ORDER TRANSITION AT $h = 0$.

In the weak coupling limit, the conventional approach is to treat the kinetic (single particle) term exactly, then treat the weak interaction term by perturbation theory. In the opposite strong coupling limit, one may treat interaction exactly, then treat the kinetic term by perturbation theory [S1]. However, in the intermediate regime, usually no controlled analytical approach can be found.

In this manuscript, we are focusing on the weak interaction $U < t_0$ regime, which is also the experimentally relevant situation. So conventional approach can be used to study the Z-FM in the $h \gg U$ limit. However, when h becomes also weak, namely, in the regime $h \lesssim U$, it becomes quite tricky and difficult to study the delicate balance between the weak interaction effects and the weak Zeeman effects. Here, we show that if one still takes the conventional (or traditional) approach which treats the kinetic (single particle) term first, then the interaction by perturbation, one reaches that there is a first order transition line at $h = 0$ (Fig.S1a). As shown in the main text, this conclusion is in-correct. This is because the conventional approach fails to capture the NOFQD effect which treats the kinetic term and interaction effects on the equal footing, so completely breaks down in this regime. A new and systematic approach is needed to capture the NOFQD effect.

Such a new approach is the GL action developed in the main text. As alerted in the first paragraph, in a general many body interacting system, it is very difficult to construct a controlled analytic approach when the two competing scales such as the kinetic energy and the interaction are comparable. Here, we make two crucial observations (1) even in the presence of h , the quantum ground state can still be chosen from the manifold spanned by the family of states shown in Eq.M2 parameterized by Eq.M4. (2) We managed to find an analytic formula for the effective potential generated by the order from disorder phenomena Eq.M5 which holds in the whole range ($0 < \theta < \pi, 0 < \phi < 2\pi$). (For the explicit derivation of this formula, see the next section of the SM). This complete formula is important, because the minimum (θ_0, ϕ_0) changes as h increases. In fact, this complete formula was also predicted independently from the symmetry based GL action.

It is these two facts which enable us to democratically and systematically capture the NOFQD effect which stands for the delicate competition between the effective potential generated by the OFQD due to the weak interaction and the Zeeman energy due to a small finite h , therefore map out the global phase diagram Fig.M1. Especially, the first order transition at $h = 0$ is transferred to the two second order transitions at $h = \pm h_c$, then a "new" phase called canted AFM phase (CAFM) emerges in the narrow window of $0 < h < h_c$ (it still has the same symmetry as the $N = 2$ XY-AFM phase). Obviously, there is a qualitative change from first order transition reached by the conventional approach which ignores the NOFQD effects and the second order transition reached by the new approach which incorporates the NOFQD effects. It is the second order transition associated with the NOFQD which leads to all the sharp experimentally detectable predictions presented in the main text.

Although this conventional approach breaks down and lead to in-correct physics at $h \lesssim U$, especially a first order transition at $h = 0$, it is still instructive to present this traditional approach in this SM, because it was used to inspire the authors to discover the NOFQD phenomena and to develop the new and systematic GL action approach in the main text to explore the NOFQD phenomena [S13]. It may also help to shed some lights on the physical implications of NOFQD phenomena on the phase diagram in Fig.M1.

(a) *The conventional approach to find the Z-FM at any $h > 0$.*

Any small $h \neq 0$ breaks the mirror symmetry and split the degenerate single-particle state at momentum $(0, 0)$ and (π, π) . A straightforward mean field analysis predicts the condensation occurs at either $(0, 0)$ or (π, π) depending on the sign of h . the unique lowest energy single-particle state lead to $|\Psi_{\text{sf}, \uparrow}\rangle \sim (\sum_i a_{i\uparrow}^\dagger)^N |0\rangle$ if $h > 0$ or $|\Psi_{\text{sf}, \downarrow}\rangle \sim [\sum_i (-1)^{i_x+i_y} a_{i\downarrow}^\dagger]^N |0\rangle$ if $h < 0$. Due to their spin alinement along the z axis, we name it $Z - FM$ superfluid.

Then after choosing $(0, 0)$ as the unique BEC condensation point at $h > 0$, we apply the Bogoliubov theory to study the effects of the interaction U at any $h \neq 0$. As shown in Sec.M2, we obtain a linear gapless superfluid mode and a gapped roton mode with the gap at $\vec{Q} = (\pi, \pi)$ listed in Eq.8

$$\Delta_R^0(h) = 2|h|$$

shown in Fig.S1b (also shown in the dash line in Fig. M4b in the main text). As one decreases h from $h \gg U$ to $h \lesssim U$, then to 0^+ , the roton mode at $\vec{Q} = (\pi, \pi)$ gets lower and lower, then touches zero at $h = 0^+$. This behaviour may signify a possible first order transition at $h_c = 0^+$. This physical picture leads to the naive phase diagram shown in Fig.S1a.

As shown in the main text, this conventional approach is valid at $h > U$, but breaks down when $h \lesssim U$. Then the next two steps

(b) *The order from quantum disorder analysis to find the $N = 2$ XY-AFM state at $h = 0$ and*

(c) *The Roton mass gap generated from the "order by disorder" mechanism in the $N = 2$ XY-AFM state st $h = 0$.* were performed in Sec.3 and Sec.4 in the main text respectively.

(d) *A naive (also wrong) Roton mass gap at $h > 0$ which ignores the NOFQD effects.*

In the conventional approach taken in (a), we treat h exactly, then treat U by perturbation. So we may expect that the roton gap at any $h \neq 0$ could be obtained simply by incorporating the roton gap Eq.13 at $h = 0$ directly into the roton gap Eq.8 at $h \neq 0$:

$$\Delta_R(h) = \sqrt{\Delta_R^2(h = 0) + 4h^2} \quad (\text{S1})$$

which is always above the dashed line and shown in the solid line in Fig.S1b.

Eq.S1 leads to the following scenario: The transition at $h = 0$ is a first order phase transition in Fig.S1a driven by the roton dropping tuned by the Zeeman field h shown in the solid line in Fig.S1b. The roton still has a non-zero gap $\Delta_R(h = 0)$ in Eq.13 before it sparks the first order transition.

Now the contradiction comes: if it were indeed a first order transition at $h = 0$, then the state would be a mixed state of the $(0, 0)$ spin up state and (π, π) spin down state with any ratio. However, by the OFQD phenomena at $h = 0$, we found the state is a pure state: the $N = 2$ XY-AFM state instead of a mixed state. This contradiction shows the conventional approach may break down when $h \rightarrow 0^+$.

Indeed, as shown in the main text, this naive scenario holds only when h is sufficiently large $h > U$, but breaks down at a small $h \lesssim U$. As explicitly demonstrated in the main text, to compute the roton spectrum at $h \lesssim U$, one must examine the NOFQD effects which treat the effects of U and h on equally footing. Namely, by treating the two nearly degenerate states at $(0, 0)$ and (π, π) on equal footing, one can investigate the competitions between the effective potential generated by the OFQD in Fig.M2 due to the interaction U and the Zeeman energy due to a small finite h . The systematic GL effective calculation developed in the main text precisely capture the NOFQD effects and

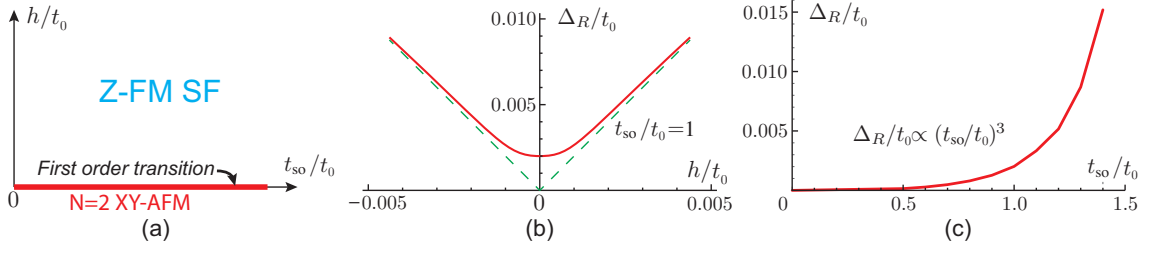


FIG. S1. (a) The naive zero temperature phase diagram as a function of t_{so}/t_0 and h/t_0 with fixed n_0U reached by the conventional approach which ignores the NOFQD effects. If ignoring the NOFQD effects, then any small $h > 0$ will select the Z-FM. So any small h would induce a first order transition from the $N = 2$ XY-AFM to the Z-FM. However, incorporating the NOFQD effects will change the naive phase diagram to the correct Fig.1a in the main text. (b) The dashed line indicates that when the OFQD effect at $h = 0$ is ignored, the roton gap drops to zero as $h \rightarrow 0^+$ as Eq.8. Then the OFQD generates the roton gap Eq.13 at $h = 0$ whose dependence on t_{so}/t_0 is given in (c). The solid line is the naively extrapolated roton gap behaviours Eq.S1 in the conventional approach. (c) At $h = 0$, the Roton gap computed by the OFQD analysis is an increasing function of t_{so} as approaching to the right. Other parameters are $n_0U = 1$, $n_0 \approx 1$. At $t_{so} = 0$, it is nothing but the FM spin wave mode. At small t_{so} , it can also be calculated by the perturbation theory in t_{so} which leads to $\Delta_R \sim t_{so}^3$ (see the next section below Eq.S24). As shown in the main text, only (c) remains correct, (a) and (b) should be replaced by Fig.M1a and Fig.M4b respectively.

leads to the correct roton spectrum in the second equation in Eq.M18 where one can extract the correct roton gap at any $h < h_c$:

$$\Delta_R^- = 4AB \sin^4 \theta_0 = 2\sqrt{B/A^3}(A^2 - n_0^2 h^2)/n_0 \quad (S2)$$

which is listed in Eq.28 and shown in the solid line in Fig.M4b. In the $h \rightarrow h_c^-$ limit, the roton gap vanishes as $\Delta_R \sim h_c - h$. Note that the new and systematic GL action approach not only leads to the correct roton gap Eq.S2, but also the correct roton spectrum at any k in the long wavelength limit in the second equation in Eq.M18 (the solid line in Fig.M3b) which is qualitatively different from the naively speculated roton spectrum Eq.S1 (the solid line in Fig.S1b).

Therefore, the breakdown of the conventional approach at $h \lesssim U$ leads to a qualitative change of the physical picture: The first order transition at $h = 0$ splits into two second order transitions at a finite $h = \pm h_c$ shown in Fig.M1a. The $N = 2$ XY-AFM SF phase at $h = 0$ turns into the canted AFM SF phase at $h > 0$. Of course, the two phases still have the same symmetry breaking patterns. It is the zero temperature 2nd order transition associated with the NOFQD effects which leads to all the sharp predictions on all the experimental measurable quantities analyzed in the main text.

In short, we demonstrate that the effective potential generated from the OFQD at least has 3 important impacts in the bosonic QAH system: (a) at $h = 0$, it leads to a quantum ground state selection rule, (b) it also opens a gap to the roton mode at $h = 0$ (c) Most importantly, at small $h \lesssim U$, it leads to the NOFQD effects. Then we develop a new and systematic GL effective action scheme to capture the NOFQD effects which stands for the competition between the effective potential generated by the "order from disorder" mechanism with the Zeeman energy due to a small finite h . The competition leads to the corrected roton excitation spectra at any k in the long wavelength limit in the second equation in Eq.M18. It is the roton gap closing at $h = h_c$ which drives a second order quantum phase transition (QPT) from the CAFM to the Z-FM in Fig.M1b. The QPT at $T = 0$ associated with the NOFQD effects leads to sharp and unique predictions in several physical quantities which can be easily detected in the current experiments.

B. THE FUNCTIONAL FORM OF THE EFFECTIVE POTENTIAL GENERATED BY THE OFQD

Here, we will explicitly demonstrate the explicit functional form Eq.M5 which holds in the whole range $0 < \theta < \pi, 0 < \phi < 2\pi$. This complete formula is important, because the minimum (θ_0, ϕ_0) changes as h increases. It is this formula which enable us to democratically and systematically capture the NOFQD effects, therefore map out the global phase diagram Fig.M1. Most importantly, this formula reached by the microscopic calculation at weak coupling precisely match the most general form in the phenomenological GL action constructed just from the symmetry principle. This match establishes the deep connection between the two independent, different, but complementary approaches.

1. Analytical approach: perturbation theory in t_{so}/t_0 .

In Fig.M1a, at small t_{so}/t_0 and $h = 0$, we perform the perturbation calculation in t_{so}/t_0 which is independent and complementary to the order from disorder analysis done in the main text. This in-dependent approach can also be used as a check on the results achieved from the order from disorder analysis.

Before performing perturbation calculations, it is convenient to apply transformation $a_{i\downarrow} \rightarrow (-1)^i a_{i\downarrow}$ to the original Hamiltonian Eq.(1) and obtain

$$\mathcal{H} = -t_0 \sum_{\langle ij \rangle} a_i^\dagger a_j + it_{\text{so}} \sum_{\langle ij \rangle} (-1)^i a_i^\dagger (d_{ij} \cdot \vec{\sigma}) a_j - h \sum_i a_i^\dagger \sigma^z a_i + \frac{U}{2} \sum_i n_i (n_i - 1) - \mu \sum_i n_i \quad (\text{S3})$$

Since the ground-state energy is a gauge invariant quantity, we can use the Hamiltonian Eq.(S1) for the ground-state energy calculation. In the absent of Zeeman field $h = 0$, we first separate Hamiltonian Eq.(S1) into two parts

$$\mathcal{H}_0 = -t_0 \sum_{\langle ij \rangle} a_i^\dagger a_j + \frac{U}{2} \sum_i n_i (n_i - 1) - \mu \sum_i n_i, \quad \mathcal{H}_{\text{so}} = it_{\text{so}} \sum_{\langle ij \rangle} (-1)^i a_i^\dagger (d_{ij} \cdot \vec{\sigma}) a_j \quad (\text{S4})$$

Because the Hamiltonian \mathcal{H}_0 has the spin $SU(2)_s$ symmetry in the rotated $\tilde{SU}(2)$ basis $\tilde{\mathbf{S}}_i = ((-1)^{i_x+i_y} S_i^x, (-1)^{i_x+i_y} S_i^y, S_i^z)$, at the weak coupling $U \ll t$ one can condense the spinor bosons at $\mathbf{k} = \mathbf{0}$ with the spin symmetry breaking direction along (θ, ϕ) . So the ground-state is a superfluid with many-body wavefunction $|\Psi_{\text{sf}}\rangle \sim (\sum \Psi_i a_i^\dagger)^N |\text{Vac}\rangle$ where $\Psi_i = c_0 \eta_0 + c_\pi \eta_\pi$ and $|c_0|^2 + |c_\pi|^2 = 1$. Notice we are using the same notation $\eta_0 = \begin{pmatrix} 1 \\ 0 \end{pmatrix}$ and $\eta_\pi = \begin{pmatrix} 0 \\ 1 \end{pmatrix}$ as defined in main text. The coefficients parameterize the same as Eq. M4 $c_0 = e^{-i\phi/2} \cos(\theta/2)$ and $c_\pi = e^{+i\phi/2} \sin(\theta/2)$.

Within Bogoliubov approximation, the original boson operators is replaced by condensate part plus a fluctuations $a_i = \sqrt{N_0} \Psi_i + \psi_i$, thus one can expand \mathcal{H}_0 and keep terms up to second order in the fluctuations. The quadratic theory of \mathcal{H}_0 after the expansion is $\mathcal{H}_{0,\text{Bog}}$, which can be diagonalized as

$$\mathcal{H}_{0,\text{Bog}} = \text{const.} + \sum_{\mathbf{k}} (\omega_{1,\mathbf{k}} \alpha_{1,\mathbf{k}}^\dagger \alpha_{1,\mathbf{k}} + \omega_{2,\mathbf{k}} \alpha_{2,\mathbf{k}}^\dagger \alpha_{2,\mathbf{k}}) \quad (\text{S5})$$

where Bogoliubov transformation is given by

$$\psi_{\mathbf{k}\uparrow} = -\bar{c}_\pi \alpha_{1,\mathbf{k}} + c_0 (\cosh \xi_{\mathbf{k}} \alpha_{2,\mathbf{k}} + \sinh \xi_{\mathbf{k}} \alpha_{2,-\mathbf{k}}^\dagger), \quad \psi_{\mathbf{k}\downarrow} = +\bar{c}_0 \alpha_{1,\mathbf{k}} + c_\pi (\cosh \xi_{\mathbf{k}} \alpha_{2,\mathbf{k}} + \sinh \xi_{\mathbf{k}} \alpha_{2,-\mathbf{k}}^\dagger) \quad (\text{S6})$$

and the excitation spectrum are $\omega_{1,\mathbf{k}} = 4t_0 - 2t_0(\cos k_x + \cos k_y)$ and $\omega_{2,\mathbf{k}} = \sqrt{\omega_{1,\mathbf{k}}(\omega_{1,\mathbf{k}} + 2n_0 U)}$. The auxiliary angle is defined as $\xi_{\mathbf{k}} = -\frac{1}{2} \text{arctanh}[\frac{\omega_{1,\mathbf{k}}}{\omega_{1,\mathbf{k}} + n_0 U}]$. The ground-state $|0\rangle$ of $\mathcal{H}_{0,\text{Bog}}$ is the vacuum of $\alpha_{1,\mathbf{k}}$ and $\alpha_{2,\mathbf{k}}$, so that $\alpha_{1,\mathbf{k}}|0\rangle = 0$ and $\alpha_{2,\mathbf{k}}|0\rangle = 0$.

The $SU(2)_s$ symmetry of \mathcal{H}_0 guaranteed that c_0 and c_π can take any values as long as they satisfy normalization condition. Namely, any spin symmetry breaking direction along (θ, ϕ) is equivalent. However, \mathcal{H}_{so} explicitly breaks the $SU(2)_s$ symmetry, so the $SU(2)_s$ symmetry becomes spurious and only exists at mean-field level.

Now the perturbation \mathcal{H}_{so} takes following form in the Bogoliubov approximation

$$\mathcal{H}_{\text{so}} = 2t_{\text{so}} \sum_{\mathbf{k}} (\gamma_{\mathbf{k}} \psi_{\mathbf{k}\uparrow}^\dagger \psi_{\mathbf{k}+\mathbf{Q}\downarrow} + h.c.) \quad (\text{S7})$$

where $\gamma_{\mathbf{k}} = \sin k_x - i \sin k_y$ and $\mathbf{Q} = (\pi, \pi)$.

In order to apply the perturbation, it is convenient to express \mathcal{H}_{so} in terms of $\alpha_{\mathbf{k}}$:

$$\begin{aligned} \mathcal{H}_{\text{so}} = t_{\text{so}} \sum_{\mathbf{k}} [& f_{1,\mathbf{k}} \alpha_{1,\mathbf{k}}^\dagger \alpha_{1,\mathbf{k}+\mathbf{Q}} + f_{2,\mathbf{k}} \alpha_{2,\mathbf{k}}^\dagger \alpha_{2,\mathbf{k}+\mathbf{Q}} + f_{3,\mathbf{k}} \alpha_{1,\mathbf{k}}^\dagger \alpha_{2,\mathbf{k}+\mathbf{Q}} + f_{4,\mathbf{k}} \alpha_{2,\mathbf{k}}^\dagger \alpha_{1,\mathbf{k}+\mathbf{Q}} \\ & + (f_{5,\mathbf{k}} \alpha_{1,\mathbf{k}}^\dagger \alpha_{2,-\mathbf{k}+\mathbf{Q}}^\dagger + f_{6,\mathbf{k}} \alpha_{2,\mathbf{k}}^\dagger \alpha_{2,-\mathbf{k}+\mathbf{Q}}^\dagger + h.c.)] \end{aligned} \quad (\text{S8})$$

where the coefficients are

$$f_{1,\mathbf{k}} = -\sin\theta(e^{i\phi}\gamma_{\mathbf{k}} - e^{-i\phi}\bar{\gamma}_{\mathbf{k}}) \quad (\text{S9})$$

$$f_{2,\mathbf{k}} = \sin\theta(\cosh\xi_{\mathbf{k}}\cosh\xi_{\mathbf{k}+\mathbf{Q}} + \sinh\xi_{\mathbf{k}}\sinh\xi_{\mathbf{k}+\mathbf{Q}})(e^{i\phi}\gamma_{\mathbf{k}} - e^{-i\phi}\bar{\gamma}_{\mathbf{k}}) \quad (\text{S10})$$

$$f_{3,\mathbf{k}} = -2\cosh\xi_{\mathbf{k}+\mathbf{Q}}[e^{i\phi}\sin^2(\theta/2)\gamma_{\mathbf{k}} + e^{-i\phi}\cos^2(\theta/2)\bar{\gamma}_{\mathbf{k}}] \quad (\text{S11})$$

$$f_{4,\mathbf{k}} = 2\cosh\xi_{\mathbf{k}}[e^{i\phi}\cos^2(\theta/2)\gamma_{\mathbf{k}} + e^{-i\phi}\sin^2(\theta/2)\bar{\gamma}_{\mathbf{k}}] \quad (\text{S12})$$

$$f_{5,\mathbf{k}} = -2\sinh\xi_{\mathbf{k}+\mathbf{Q}}[e^{i\phi}\sin^2(\theta/2)\gamma_{\mathbf{k}} + e^{-i\phi}\cos^2(\theta/2)\bar{\gamma}_{\mathbf{k}}] \quad (\text{S13})$$

$$f_{6,\mathbf{k}} = \sin\theta\cosh\xi_{\mathbf{k}}\sinh\xi_{\mathbf{k}+\mathbf{Q}}(e^{i\phi}\gamma_{\mathbf{k}} - e^{-i\phi}\bar{\gamma}_{\mathbf{k}}) \quad (\text{S14})$$

By treating t_{so}/t_0 as a small parameter, one can apply perturbation theory to obtain

$$E_{\text{ofd}} = \delta E^{(1)} + \delta E^{(2)} + \delta E^{(3)} + \delta E^{(4)} + \mathcal{O}(t_{\text{so}}^5) \quad (\text{S15})$$

where we denote $\delta E^{(n)} \propto t_{\text{so}}^n$. Since \mathcal{H}_{so} has odd parity, so all odd order terms vanish and

$$\delta E^{(2)} = \langle 0 | \mathcal{H}_{\text{so}} g \mathcal{H}_{\text{so}} | 0 \rangle \quad (\text{S16})$$

$$\delta E^{(4)} = \langle 0 | \mathcal{H}_{\text{so}} g \mathcal{H}_{\text{so}} g \mathcal{H}_{\text{so}} g \mathcal{H}_{\text{so}} | 0 \rangle - \langle 0 | \mathcal{H}_{\text{so}} g \mathcal{H}_{\text{so}} | 0 \rangle \langle 0 | \mathcal{H}_{\text{so}} g^2 \mathcal{H}_{\text{so}} | 0 \rangle \quad (\text{S17})$$

where $g = \sum_{n \neq 0} \frac{|n\rangle\langle n|}{-E_n}$.

After a substitution of \mathcal{H}_{so} in Eq.S8, we reach

$$\delta E^{(2)} = -t_{\text{so}}^2 \sum_{\mathbf{k}} \left[\frac{|f_{5,\mathbf{k}}|^2}{\omega_{1,\mathbf{k}} + \omega_{2,\mathbf{Q}-\mathbf{k}}} + \frac{|f_{6,\mathbf{k}}|^2 + f_{6,\mathbf{k}}\bar{f}_{6,\mathbf{Q}-\mathbf{k}}}{\omega_{2,\mathbf{k}} + \omega_{2,\mathbf{Q}-\mathbf{k}}} \right] \quad (\text{S18})$$

and

$$\begin{aligned} \delta E^{(4)} = & -t_{\text{so}}^4 \sum_{\mathbf{k}} \left[\frac{|f_{3,-\mathbf{k}}f_{5,\mathbf{k}}|^2}{\omega_{1,\mathbf{k}}(\omega_{1,\mathbf{k}} + \omega_{2,\mathbf{Q}+\mathbf{k}})^2} + \frac{1}{\omega_{2,\mathbf{k}}} \left| \frac{f_{4,\mathbf{Q}+\mathbf{k}}f_{5,\mathbf{Q}+\mathbf{k}}}{\omega_{1,\mathbf{Q}+\mathbf{k}} + \omega_{2,\mathbf{k}}} + \frac{f_{2,-\mathbf{k}}(f_{6,\mathbf{k}} + f_{6,\mathbf{Q}-\mathbf{k}})}{\omega_{2,\mathbf{k}} + \omega_{2,\mathbf{Q}-\mathbf{k}}} \right|^2 \right. \\ & \left. + \frac{1}{\omega_{1,\mathbf{k}} + \omega_{2,\mathbf{k}}} \left| \frac{f_{1,\mathbf{k}}f_{5,\mathbf{Q}+\mathbf{k}}}{\omega_{1,\mathbf{Q}+\mathbf{k}} + \omega_{2,\mathbf{k}}} + \frac{f_{2,-\mathbf{k}}f_{5,\mathbf{Q}+\mathbf{k}}}{\omega_{1,\mathbf{k}} + \omega_{2,\mathbf{Q}-\mathbf{k}}} + \frac{f_{3,\mathbf{k}}f_{6,-\mathbf{k}}}{\omega_{2,-\mathbf{k}} + \omega_{2,\mathbf{Q}+\mathbf{k}}} + \frac{f_{3,\mathbf{k}}f_{6,\mathbf{Q}+\mathbf{k}}}{\omega_{2,\mathbf{Q}+\mathbf{k}} + \omega_{2,\mathbf{k}}} \right|^2 \right] + \dots \quad (\text{S19}) \end{aligned}$$

where \dots means ϕ -independent part.

After some manipulations, we found

$$\delta E^{(2)} = t_{\text{so}}^2 N_s [c_2 + a(1 + \cos 2\theta)], \quad (\text{S20})$$

$$\delta E^{(4)} = t_{\text{so}}^4 N_s [c_4 + b \sin^4 \theta (1 + \cos 4\phi) + \dots], \quad (\text{S21})$$

where \dots also contains θ -only dependent terms like $\cos 2\theta$ and $\cos 4\theta$ which is subleading to $\delta E^{(2)}$ when $t_{\text{so}} \ll t$. The coefficients are

$$a = \frac{1}{N_s} \sum_{\mathbf{k}} |\gamma_{\mathbf{k}}|^2 \left(\frac{\cosh^2 \xi_{\mathbf{k}} \sinh^2 \xi_{\mathbf{Q}+\mathbf{k}} + \cosh \xi_{\mathbf{k}} \sinh \xi_{\mathbf{k}} \cosh \xi_{\mathbf{Q}+\mathbf{k}} \sinh \xi_{\mathbf{Q}+\mathbf{k}}}{\omega_{2,\mathbf{k}} + \omega_{2,\mathbf{Q}+\mathbf{k}}} - \frac{\sinh^2 \xi_{\mathbf{Q}+\mathbf{k}}}{\omega_{1,\mathbf{k}} + \omega_{2,\mathbf{Q}+\mathbf{k}}} \right) \quad (\text{S22})$$

$$\begin{aligned} b = & \frac{1}{N_s} \sum_{\mathbf{k}} (\gamma_{\mathbf{k}}^4 + \bar{\gamma}_{\mathbf{k}}^4) \left[-\frac{\sinh^2(2\xi_{\mathbf{k}+\mathbf{Q}})}{4\omega_{1,\mathbf{k}}} - \frac{1}{4\omega_{2,\mathbf{k}}} \left(\frac{\sinh(2\xi_{\mathbf{k}})}{\omega_{1,\mathbf{k}+\mathbf{Q}} + \omega_{2,\mathbf{k}}} - \frac{\sinh(2\xi_{\mathbf{k}} + 2\xi_{\mathbf{k}+\mathbf{Q}})}{\omega_{2,\mathbf{k}+\mathbf{Q}} + \omega_{2,\mathbf{k}}} \right)^2 \right. \\ & \left. + \frac{1}{\omega_{1,\mathbf{k}} + \omega_{2,\mathbf{k}}} \left(\frac{\sinh(\xi_{\mathbf{k}})}{\omega_{1,\mathbf{k}+\mathbf{Q}} + \omega_{2,\mathbf{k}}} + \frac{\sinh(\xi_{\mathbf{k}+\mathbf{Q}}) \cosh(\xi_{\mathbf{k}} + \xi_{\mathbf{k}+\mathbf{Q}})}{\omega_{1,\mathbf{k}} + \omega_{2,\mathbf{k}+\mathbf{Q}}} + \frac{\cosh(\xi_{\mathbf{k}+\mathbf{Q}}) \sinh(\xi_{\mathbf{k}} + \xi_{\mathbf{k}+\mathbf{Q}})}{\omega_{2,\mathbf{k}} + \omega_{2,\mathbf{k}+\mathbf{Q}}} \right)^2 \right] \quad (\text{S23}) \end{aligned}$$

For $U > 0$ case, we can prove that $a, b > 0$. So $\delta E^{(2)}$ and $\delta E^{(4)}$ reach the minima at $\cos 2\theta = -1$ and $\cos 4\phi = -1$ respectively, which tells the quantum ground-state sits at $\theta = \pi/2$ and $\phi = \pi/4$ which are nothing but the XY-FM state. Transforming it back from the rotated $\tilde{S}\tilde{U}(2)$ basis to the original basis, it is nothing but the $N = 2$ XY-AFM SF state. So we reach the same ground state from the two independent methods.

When comparing Eq.S21 with Eq.M5,

$$E_{\text{ofd}} = E_{\text{ofd},0} + N_s \left[\frac{A}{4}(1 + \cos 2\theta) + \frac{B}{16} \sin^4 \theta (1 + \cos 4\phi) \right] + \dots \quad (\text{S24})$$

where the \dots means the higher order terms respecting the same symmetry of the Hamiltonian.

Then we obtain the analytical expressions of $A = a(2t_{\text{so}})^2$ and $B = b(2t_{\text{so}})^4$ from the perturbation theory. Then Eq.13 leads to $\Delta_R \sim t_s^3$ at $h = 0$ shown in Fig.S1b. As shown in the main text, Eq.S24 acn be written as the form in the GL action:

$$\frac{A}{2}(|\psi_1|^2 - |\psi_2|^2)^2 + \frac{B}{2}[(\psi_1^* \psi_2)^2 + (\psi_1 \psi_2^*)^2] + C(|\psi_1|^2 - |\psi_2|^2)^4 + D[(\psi_1^* \psi_2)^2 + (\psi_1 \psi_2^*)^2]^4 + \dots \quad (\text{S25})$$

where \dots means the even higher order terms than C and D term respecting the $[C_4 \times C_4]_D$ symmetry of the Hamiltonian. In fact, as shown below, the C and D terms can also be determined numerically by the microscopic calculations. Both found to be positive.

2. Numerical approach: compared with the analytical results

We will show that although the form Eq.(S24) is obtained from the perturbation theory in a small t_{so}/t_0 , its form fits numerical data very well even upto $t_{\text{so}}/t_0 = 1$. The data is obtained from numerical evaluation $\omega_{l,\mathbf{k}}$ and $E_{\text{ofd}}(\theta, \phi)$ in Eq.M3.

The comparison consist of two parts: the global property and the local property.

For the global property, we plot numerical results from Eq.M3 and the analytical result from Eq.(S24) in Fig.S2. It is clear that the two results fit quite well in the whole range $0 < \theta < \phi, 0 < \phi < \pi/2$.

On the other hand, if we only keep the form of the perturbation theory and treat coefficients A and B as fitting parameters, then the relative error can be controlled below 1%. Figure S2 shows the form work very well even for t_{so} is not small, i.e. $t_{\text{so}}/t = 1$.

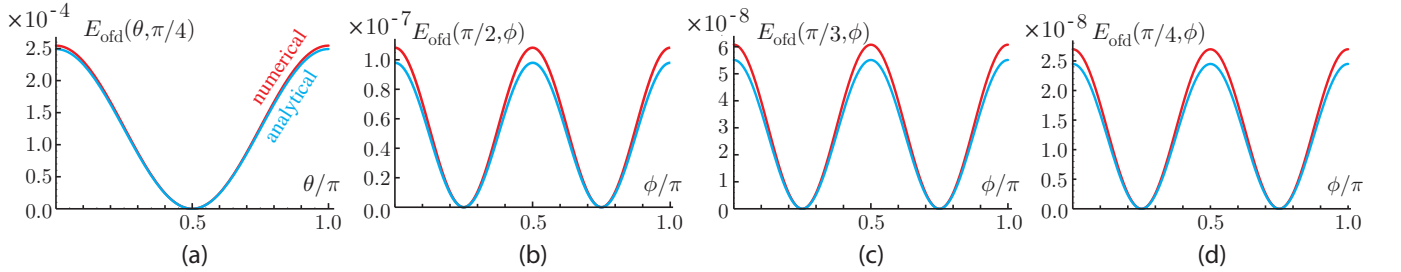


FIG. S2. Plot of E_{ofd} for varies parameter regimes (a) $0 < \theta < \pi$ and $\phi = \pi/4$, (b) $\theta = \pi/2$ and $0 < \phi < \pi$, (c) $\theta = \pi/3$ and $0 < \phi < \pi$, (d) $\theta = \pi/4$ and $0 < \phi < \pi$. The numerical results are represented by the red lines, and the analytical results from the perturbation theory are represented by the blue lines. The other parameters are $t_{\text{so}}/t = 1/3$, $n_0 U/t_0 = 1$.

In fact, the higher order terms such as $(|\psi_1|^2 - |\psi_2|^2)^4$ and $[(\psi_1^* \psi_2)^2 + (\psi_1 \psi_2^*)^2]^4$ in Eq.(S25) can also be determined from Fig.S2. The fact that the period of ΔE is only half of E can be cast into these high-order terms. For example, the 4th order perturbation also contain θ -only dependent terms like $\cos 2\theta$ and $\cos 4\theta$, but they are proportional to t_{so}^4 . The $\cos 2\theta$ terms do not change the form of Eq.(S25), they can be absorbed into the coefficient A anyway. But $\cos 4\theta$ does. So after the subtraction, only small sub-leading terms survive, then $\Delta E(\theta, \pi/4) \sim \cos 4\theta$ can be cast into the form $C(|\psi_1|^2 - |\psi_2|^2)^4$. Similar arguments hold also for ϕ and lead to $\Delta E(\pi/2, \phi) \sim \cos 8\phi$ which can be cast into $D[(\psi_1^* \psi_2)^2 + (\psi_1 \psi_2^*)^2]^4$. Both C and D are found to be positive.

For the local property, we focus on the derivative with respect to θ and ϕ :

$$A'(\theta_0) = \frac{\partial^2}{\partial \theta^2} E_{\text{ofd}}(\theta, \phi) \Big|_{\theta=\theta_0, \phi=\pi/4}, \quad B'(\theta_0) = \frac{\partial^2}{\partial \phi^2} E_{\text{ofd}}(\theta, \phi) \Big|_{\theta=\theta_0, \phi=\pi/4} \quad (\text{S26})$$

Analytical result Eq.(S24) predicts $A'_{\text{an}} = -A \cos 2\theta_0$ and $B'_{\text{an}} = B \sin^4 \theta_0$, and numerical derivatives can be evaluated from the finite differences of Eq.M3. We plot both results in Fig.S3(a) and (b), and find the differences are quite small. The insert of Fig.S3(b) also confirms $B' \sim \theta^4$ behaviour.

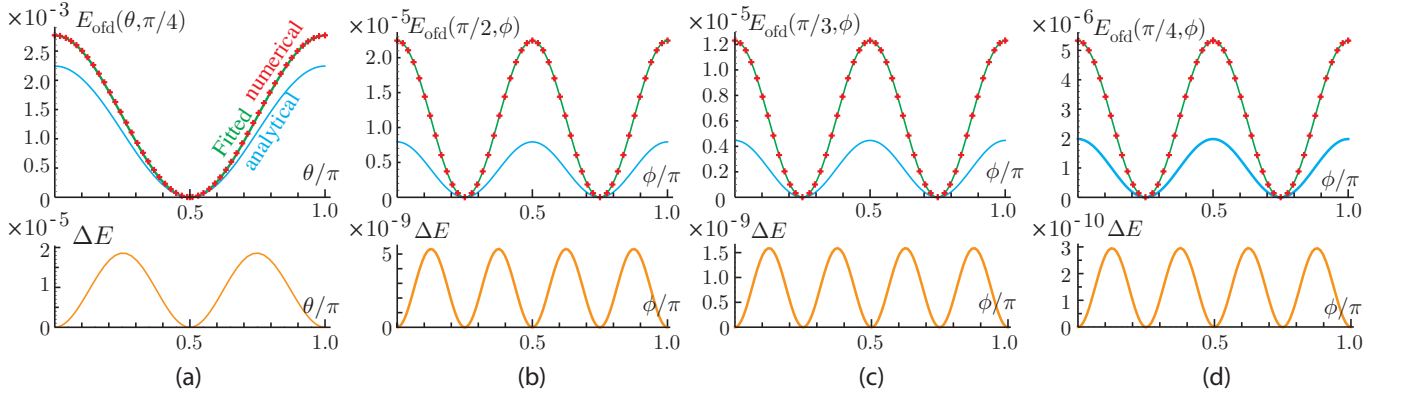


FIG. S3. The same as Fig.S2 except using different parameters $t_{so}/t = 1$, $n_0 U/t_0 = 1$. The numerical results are represented by the red + symbol, the analytical results from the perturbation theory are represented by the blue lines, and fitting results are represented by the green lines (namely, treating coefficients A and B just as fitting parameters). The difference between the numerical results and the fitting results $\Delta E = E_{\text{numerical}} - E_{\text{fit}}$ are listed below each sub-figure to show the form of Eq.(S24) is still very accurate even at large $t_{so}/t = 1$.

As a final comparison, we evaluate A' and B' as a function of t_{so} and plot them in Fig.S3(c) and (d). When extrapolating the data to the $t_{so} \rightarrow 0$ limit, they reach agreement with the perturbation results with a high accuracy. The insert of Fig.S3 (c) and (d) also shows that the leading behaviours of $A' \sim t_{so}^2$ and $B' \sim t_{so}^4$, in consistent with the perturbation theory listed below Eq.eq:pb.

In conclusion, we show that the E_{ofd} obtained from the perturbation theory fit very well the data from the direct numerical evaluations, even upto $t_{so}/t = 1$.

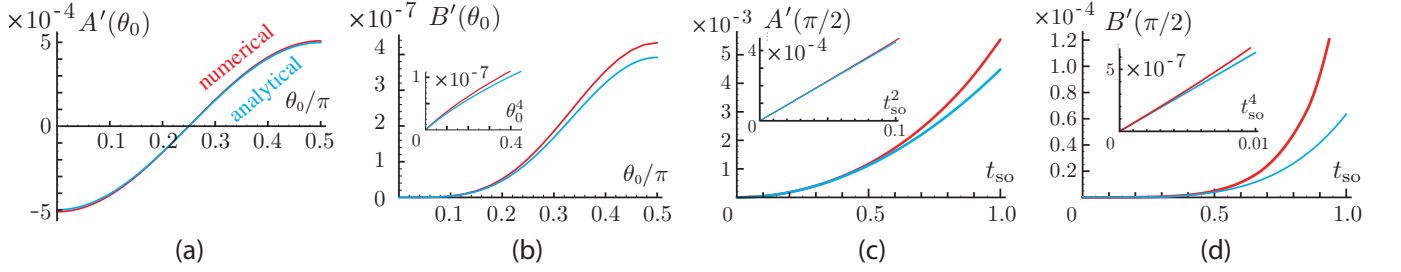


FIG. S4. (a) Coefficient A' as a function of θ_0 , (b) Coefficient B' as a function of θ_0 , The insert shows $B' \sim \theta_0^4$ when θ_0 is small. (c) Coefficient A' as a function of t_{so} , The insert shows $A' \sim t_{so}^2$ when t_{so} is small. (d) Coefficient B' as a function of t_{so} . The insert shows $B' \sim t_{so}^4$ when t_{so} is small.

C. SOME ADDITIONAL CALCULATIONS USING THE EFFECTIVE GL ACTION

In this appendix, we will use the effective action Eq.21 to perform alternative calculations to compute the excitation spectrum in both $h > h_c$ and $h < h_c$. They reproduce the results Eq.31 and Eq.27 respectively achieved in the main text and also provide additional physical insights into the problem.

1. A rotated polar coordinate calculation at $h > h_c$

When $h > h_c$, the system is in the Z-FM superfluid phase with the saddle point solution Eq.24 $\bar{\rho}_1 = \rho_0 = -r/U$, $\bar{\rho}_2 = 0$, and no constraints on $\bar{\theta}_1$ and $\bar{\theta}_2$. In order to avoid any singularities in using the polar coordinates, we introduce two rotated order parameters:

$$\psi'_1 = (\psi_1 + \psi_2)/\sqrt{2}, \quad \psi'_2 = (\psi_1 - \psi_2)/\sqrt{2} \quad (\text{S27})$$

then parameterize them as $\psi'_1 = \sqrt{\rho'_1}e^{i\theta'_1}$ and $\psi'_2 = \sqrt{\rho'_2}e^{i\theta'_2}$. It is easy to identify the saddle point solution $\bar{\rho}_1 = \rho_0, \bar{\rho}_2 = 0, \bar{\theta}_1 = \bar{\theta}_2 = 0$ in old coordinates system correspond to $\bar{\rho}'_1 = \bar{\rho}'_2 = \rho_0/2, \bar{\theta}'_1 = \bar{\theta}'_2 = 0$ in new coordinate system.

For the notation simplicity, in the following, we drop the ' in ρ and θ . After including fluctuations as $\psi_\alpha = \sqrt{\rho_\alpha + \delta\rho_\alpha}e^{i(\bar{\theta}_\alpha + \delta\theta_\alpha)}$, then

$$\begin{aligned} \mathcal{L}_{ZF} = & i\delta\rho_1\partial_\tau\delta\theta_1 + i\delta\rho_2\partial_\tau\delta\theta_2 + \frac{v^2}{2\rho_0}[(\nabla\delta\rho_1)^2 + (\nabla\delta\rho_2)^2] + \frac{1}{2}v^2\rho_0[(\nabla\delta\theta_1)^2 + (\nabla\delta\theta_2)^2] \\ & + \frac{U}{2}(\delta\rho_1 + \delta\rho_2)^2 + \frac{A}{2}[4\delta\rho_1\delta\rho_2 - \rho_0^2(\delta\theta_1 - \delta\theta_2)^2] + \frac{h}{2}[\frac{1}{\rho_0}(\delta\rho_1 - \delta\rho_2)^2 + \rho_0(\delta\theta_1 - \delta\theta_2)^2] \end{aligned} \quad (\text{S28})$$

where the linear term drops out due to the saddle point condition $[r + (A + U)\rho_0 - h](\delta\rho_1 + \delta\rho_2) = 0$. From Eq.(S28), one can easily extract two eigen-modes in the long wavelength limit:

$$\omega_- = \sqrt{2\rho_0(A + U)v^2k^2} \quad (\text{S29})$$

$$\omega_+ = 2(h - A\rho_0) + v^2k^2 \quad (\text{S30})$$

which are identical to Eq.31.

Similar to Eq.26, one can also introduce \pm in the new coordinates system: $\delta\rho_\pm = \delta\rho_1 \pm \delta\rho_2$ and $\delta\theta_\pm = \delta\theta_1 \pm \delta\theta_2$, then

$$\begin{aligned} \mathcal{L}_{FM} = & \frac{i}{2}\delta\rho_+\partial_\tau\delta\theta_+ + \frac{v^2}{4\rho_0}[(\nabla\delta\rho_+)^2 + \rho_0^2(\nabla\delta\theta_+)^2] + \frac{A + U}{2}(\delta\rho_+)^2 \\ & + \frac{i}{2}\delta\rho_-\partial_\tau\delta\theta_- + \frac{v^2}{4\rho_0}[(\nabla\delta\rho_-)^2 + \rho_0^2(\nabla\delta\theta_-)^2] + \frac{h - A\rho_0}{2\rho_0}[(\delta\rho_-)^2 + \rho_0^2(\delta\theta_-)^2] \end{aligned} \quad (\text{S31})$$

which lead to exactly the same two eigen-modes.

2. A mixed coordinate calculation at $h < h_c$

One may also use the mixed coordinate system representation to calculate the excitation spectrum in the CAFM SF at $h < h_c$. Namely, using the saddle point in Eq.23 and substituting $\psi_1 = \sqrt{\bar{\rho}_1 + \delta\rho_1}e^{i(\bar{\theta}_1 + \delta\theta_1)}$ and $\psi_2 = \sqrt{\bar{\rho}_2}e^{i\bar{\theta}_2} + \delta\psi_2$ into Eq.21 leads to the quadratic part of the Lagrangian:

$$\begin{aligned} \mathcal{L}_{CA} = & i\delta\rho_1\partial_\tau\delta\theta_1 + \delta\psi_2^*\partial_\tau\delta\psi_2 + \frac{v^2}{4\rho_1}(\nabla\delta\rho_1)^2 + v^2\bar{\rho}_1(\nabla\delta\theta_1)^2 + v^2|\nabla\delta\psi_2|^2 + (r + h)|\delta\psi_2|^2 \\ & + \frac{1}{2}(U + A)(\delta\rho_1)^2 + 8B\rho_1^2\rho_2^2(\delta\theta_1)^2 + [2(U + A)\rho_2 + (U - A)\rho_1 + 4B\rho_1^2\rho_2]|\delta\psi_2|^2 \\ & - i[\frac{1}{2}(U + A) - 2B\rho_1^2]\rho_2(\delta\psi_2)^2 + i[\frac{1}{2}(U + A) - 2B\rho_1^2]\rho_2(\delta\psi_2^*)^2 \\ & + (U - A)\rho_2^{1/2}\delta\rho_1(e^{-i\pi/4}\delta\psi_2 + e^{+i\pi/4}\delta\psi_2^*) + 8B\rho_1^2\rho_2^{3/2}\delta\theta_1(e^{+i\pi/4}\delta\psi_2 + e^{-i\pi/4}\delta\psi_2^*) \end{aligned} \quad (\text{S32})$$

From Eq.(S32), one can extract the two eigen modes which are exactly the same as Eq.27 obtained in the polar coordinates in the main text.

[S1] For the conventional strong-coupling approach in a SOC system, see Fadi Sun, Jinwu Ye, Wu-Ming Liu, Quantum magnetism of spinor bosons in optical lattices with synthetic non-Abelian gauge fields at zero and finite temperatures, Phys. Rev. A 92, 043609 (2015).

[S2] To calculate the gap at $h = 0$, this expansion of the effective potential near the minimum $\theta = \pi/2, \phi = \pi/4$ is enough. However, to get the correct roton spectrum at any $h > 0$ at any k in the long wavelength limit, one need to find the complete form of the the effective potential in all ranges of $0 < \theta < \pi, 0 < \phi < 2\pi$ which is found to be Eq.M5 and re-written as Eq.M6 in the main text. Most importantly, as shown in the main text, just from the symmetry point of view, the A term and B term in the phenomenological GL action Eq.21 precisely match Eq.M6 at the weak coupling limit. This endows the effective potential generated by OFQD from a new and profound perspective.